NON-DESTRUCTIVE EVALUATION OF RESIDUAL STRESSES IN THE MULTI-PASS STEEL WELDMENTS

A THESIS SUBMITTED TO
THE GRADUATE SCHOOL OF NATURAL AND APPLIED SCIENCES
OF
MIDDLE EAST TECHNICAL UNIVERSITY

BY

GÖKHAN ERİAN

IN PARTIAL FULFILLMENT OF THE REQUIREMENTS
FOR
THE DEGREE OF MASTER OF SCIENCE
IN
METALLURGICAL AND MATERIALS ENGINEERING

AUGUST 2012

Approval of the thesis

NON-DESTRUCTIVE EVALUATION OF RESIDUAL STRESSES IN THE MULTI-PASS STEEL WELDMENTS

Submitted by **GÖKHAN ERİAN** in partial fulfillment of the requirements for the degree of **Master of Science in Metallurgical and Materials Engineering Department, Middle East Technical University** by

Prof. Dr. Canan Özgen
Dean, Graduate School of **Natural and Applied Sciences** _____

Prof. Dr. C. Hakan Gür
Head of Department, **Metallurgical and Materials Eng.** _____

Prof. Dr. C. Hakan Gür
Supervisor, **Metallurgical and Materials Eng. Dept., METU** _____

Dr. Caner Batıgün
Co-Supervisor, **Weld. Tech. and NDT Res./App. C., METU** _____

Examining Committee Members

Prof. Dr. Cevdet Kaynak
Metallurgical and Materials Eng. Dept., METU _____

Prof. Dr. C. Hakan Gür
Metallurgical and Materials Eng. Dept., METU _____

Assist. Prof. Dr. Y. Eren Kalay
Metallurgical and Materials Eng. Dept., METU _____

Assist. Prof. Dr. Caner Şimşir
Manufacturing Eng. Dept., Atılım U. _____

Dr. Caner Batıgün
Welding Tech. and NDT Res./App. C., METU _____

Date: 28/08/2012

I hereby declare that all information in this document has been obtained and presented in accordance with academic rules and ethical conduct. I also declare that, as required by these rules and conduct, I have fully cited and referenced all material and results that are not original to this work.

Name, Last name: Gökhan ERİAN

Signature:

ABSTRACT

NON-DESTRUCTIVE EVALUATION OF RESIDUAL STRESSES IN THE MULTI-PASS STEEL WELDMENTS

Erian Gökhan

M. Sc., Department of Metallurgical and Materials Engineering
Supervisor : Prof. Dr. C. Hakan Gür
Co-supervisor : Dr. Caner Batıgün

August 2012, 68 Pages

The purpose of this thesis is non-destructive determination of residual stress state in the multi-pass welded steel plates by Magnetic Barkhausen Noise (MBN) technique. To control the effectiveness of the developed procedure, continuous MBN measurements on the heat affected zone and parent metal of the welded plates were performed. In the experimental part, various steel plates were welded with different number of weld passes. Various series of samples were prepared for residual stress and for angular deflection measurements. Microstructural investigation and hardness measurements were also conducted. The results were discussed to evaluate the effectiveness of MBN measurements to monitor the changes in the residual stress state in the welded components as a function of weld pass number.

Keywords: Steel, Residual Stress, Non-destructive Evaluation, Magnetic Barkhausen Noise, Effect of Weld Passes

ÖZ

ÇOKLU PASO YAPILARAK KAYNAKLANMIŞ ÇELİKLERDE KALINTI GERİLMELERİN TAHRİBATSIZ YÖNTEMLERLE BELİRLENMESİ

Erian Gökhan

Yüksek Lisans, Metalürji ve Malzeme Mühendisliği Bölümü
Tez Yöneticisi : Prof. Dr. Dr. C. Hakan Gür
Ortak Tez Yöneticisi : Dr. Caner Batıgün

Ağustos 2012, 68 Sayfa

Bu tezin amacı çoklu paso yapılarak kaynaklanmış çeliklerde, kalıntı gerilmelerin Manyetik Barkhausen Noise (MBN) tekniği ile tahribatsız olarak ölçülmesidir. Geliştirilen yöntem kullanılarak kaynaklanmış plakalarda ısıdan etkilenen bölgede (HAZ) ve ana metalde sürekli şekilde MBN ölçümleri yapılmıştır. Deneysel kısımda çelik plakalar çoklu paso yapılarak kaynaklanmıştır. Sonra, kaynaklanmış durumda kalıntı gerilimi ölçümü ve açısal sapma miktarı ölçümleri uygulanmıştır. Mikroyapı incelemesi ve sertlik ölçümleri yapılmıştır. Elde edilen sonuçlar karşılaştırılarak, MBN yönteminin kaynaklı parçalarda kalıntı gerilmelerin kaynak paso sayısına bağlı olarak değişimin izlenmesi için uygunluğu ve verimliliği irdelenmiştir.

Anahtar Kelimeler: Çelik, Kalıntı Gerilme, Tahribatsız Muayene, Manyetik Barkhausen Gürültüsü, Kaynak Paso Sayısının Etkisi

To my father

ACKNOWLEDGEMENTS

I would like to express my deepest graduate to my thesis supervisor Prof. Dr. C. Hakan Gür for his valuable guidance, understanding, supervision and continuous support throughout the study.

I would like to thank to my thesis co-supervisor Dr. Caner Batıgün for leading and supporting me all through the study.

I would also like to express my deepest gratitude to Dr. İbrahim Çam, for his marvelous patience, guidance, criticism throughout the Barkhausen Noise measurements and also would like to thank to Central Laboratory for providing the laboratory facilities.

I would also like to thank to Assist. Prof. Dr. Caner Şimşir and Metal Forming Center of Excellence for X-ray measurements.

My special thanks go to all the members of METU Welding Technology and Non-Destructive Testing Research and Application Center for creating limitless opportunities for my studies and for their priceless efforts.

I would like to respectfully thank to Dr. Süha Tirkeş, Koray Yurtışık, Tolga Ertürk and Ahmet Taşan for guidance, encouragement, helps, advice, and acumen throughout the research.

I owe deepest gratitude to Okan Müderrisoğlu for his invaluable guidance and encouragements.

I am heartily thankful to Şaban Karakoç for his support and encouragement throughout the research.

I am also sincerely thankful to Cahit Kocaman for his modest understanding helps, advice.

I also want to thank to Melih Karamuk, Nazan Uzun, Serhan Göynük, İbrahim Arıcı for their helps and support throughout the research.

I also appreciate valuable efforts of Hakan Yurtkoruyan and Cihangir Yılmaz for their efforts and helps on machining procedure of the research.

I want to thank Utku Burgaz, Barış Yigit Alpay, Sadık Yetkin, Şükrü Kılık and Mehmet Ali Recai Önal for their friendship, help and support and especially their valuable sharing of the good and bad times of the path.

I want to thank to my aunt Yurdanur Alpman for her spiritual support throughout the all levels of the research.

I want to thank to my grandmother Afife İşgüden for sharing the load on me walking this path.

Finally I would like to express my deepest gratitude to my mother Mahinaz Erian for her unconditional and deep love, infinite support, patience and encouragement to continue.

TABLE OF CONTENTS

LIST OF TABLES

TABLES

LIST OF FIGURES

FIGURES

CHAPTER 1

INTRODUCTION

1.1 General

It is clear that as a result of world's dramatically increased energy consumption, ways to transport the combustibles gain so much importance than ever. Importance of high strength steels for pipeline, transporting petroleum and natural gas, has increased. Since these pipelines are used for long-distance, high-pressure gas and petroleum transportation via pipeline needs industrial standard codes to provide safe and sound solutions. American Petroleum Institute (API) forms technical specifications for variety of applications and environmental conditions [1].

As maximum operating pressures of pipelines are doubled standard grade of pipe steel increased from API 5L X-52 to API 5L X-70 as well. Not only number of steel grades has changed but also compositions are slightly changed. New lower carbon Mo-Ni-Ti microalloying system has taken the place of former Nb-V system. Considering the economical statue of the world, the dramatic increase at the cost of alloying elements like Mo and V makes steel producers to reduce the levels of these elements or lean on to other possibilities [2].

Controlled rolling and strain hardening are the main part of production route of API 5L X70 to form the steel for pipeline applications [3]. Yield strength of 485 MPa and tensile strength of 570 MPa must be acquired in order to satisfy the standards requirements [1]. High strength and toughness are the superior parameters of API 5L steel. This is obtained by precise chemical composition and fine grain structure through the production. Microalloying elements such as Nb are the key point to satisfy these needs. But as a production technique, thin slab casting with desired

chemical composition for API 5L X-70 grade steel is a very vulnerable procedure to slab transverse cracking with those microalloyed steel compositions that are close to peritectic range [4].

Welding is the primary procedure to form and connect pipe parts from coil or plate. Coil is cut through its length and edges are cut lengthwise. Finally they are formed at pipe mills with suitable welding techniques depending on the pipe's steel grade [5]. Several welding process, such as shielded metal arc welding (SMAW), self-shielded flux cored arc welding (FCAW-S) and gas metal arc welding (GMAW) are used for API steel series to satisfy standard codes. As design criteria not only combination of toughness and strength is needed, but also lower welding time with decreasing the number of weld passes is a must to control the cost. API steel series used for piping applications are beneficial for reducing the cost because it allows thinner wall sections and lower welding time [6]. Reducing the cost by decreasing the level of alloying element is not related to cost efficiency all the time, such as decreasing Mn level, avoids centerline segregation and decrease the harmful effects of MnS inclusions on transverse Charpy energy levels and enhance mechanical properties [2].

Residual stress formation due to primary and secondary processes through all steps of manufacturing is detrimental for the mechanical properties and has adverse effect on the life time of pipeline. As a characteristic property of welding operation, it is clear that material is affected by extreme thermal gradient and that thermal gradient develops strain both in base metal and weld metal regions. Due to the developed strain, residual stresses and distortion are presented. Thermal gradient is also responsible for undesired microstructures considering the mechanical performance. It is noticeable that joining sites of base metal and weld metal act as a stress concentrator and it is a possible candidate for a place to material fracture [7]. Also undesired wrapping of the sections can be occurred during welding. Important parameters to control and avoid undesired distortion are heat input, welding travel speed during welding sequence [8]. Beyond these parameters number of weld passes plays a key role to determine distortion and residual state characteristic of material [9].

To measure residual stress destructive methods (hole drilling technique, sectioning method and contour method are the most common ones) and non-destructive methods (X-ray diffraction, neutron diffraction method, ultrasound and magnetic Barkhausen noise method) are used [7].

To determine residual stress Magnetic Barkhausen Noise (MBN) is a promising method with its higher accuracy (±25 MPa) as compared to conventional destructive residual stress measurement when proper calibration procedure provided [10]. Measurement depth of MBN is higher compared to X-ray diffraction and also it does not need surface preparation for measurement [11]. While considering non-conventional methods, MBN is more sensitive to microstructural changes compared to ultrasound method [12].

1.2 Literature Review

E.J. McDonald et al. conducted a survey on low alloy ferritic CrMoV steel plates to see the effect of multi-pass weld repairs on residual stress. They used X-ray diffraction method for residual stress measurement and deep hole drilling techniques to do correlation. They found that maximum tensile residual stress is at the interface between heat affected zone (HAZ) and the weld metal [13].

Dean Deng and Hidekazu Murakawa studied on residual stress states in multi-pass welds of stainless steel (SUS304) pipe with thickness of 6mm and outer diameter of 114.3mm. They gathered that axial residual stress from inside and outside the pipe surface were in conflict with each other. On the inner surface of the weld zone tensile residual stress was measured however, it was compressive on the outer surface. And also on the inner surface away from the weld zone compressive residual stress was measured however, it was tensile on the outer surface [14].

I. Sattari-Far and M.R. Farahani were studied on residual stresses state in butt-welded pipes. The residual stresses measurements are conducted by the Hole-Drilling method. The pipes with wall thickness of 6mm and 10mm were used. In 10 mm pipes they concluded that on inner surface of the pipe, increasing number of weld passes increases the axial tensile stress. And also found that at the weld center line of 10 mm pipe residual stress increases with decreasing number of passes [9].

Zeng et al. studied on the relationship between the residual stress and distortion in discontinuous welding of 5A06 aluminum alloy. They concluded that angular distortion is strongly related to temperature gradient along the thickness of the body. They also stated that as a result of discontinuous welding, resulting pre-heating and reheating, angular distortion decreases [15].

Research conducted on Barkhausen Noise (BN) by Jagadish et al. unveiled the relationship between uniaxial stress and RMS voltage. As material was in tension RMS voltage increased and as it was in compression RMS voltage decreased. Magnetic parameters such as number of BN pulse and pulse height distribution was affected by stress state of the material [16].

A study done by Seppo Tiitto and Seppo Saynajakangas on spectral damping in BN revealed that BN method has effective penetration depth of 0.3mm [17]. After that for a commercial X-70 pipeline, Clapham et al. used a band-pass filter (3-200 kHz) and determined effective skin depth for MBN signal between 0.02 and 0.30 mm [18].

A study done by Gauthier et al. on steel beam to determine surface residual stress with magnetic Barkhausen Noise revealed that surface stress could be measured with MBN method. As long as a proper calibration was established, measurement was done with accuracy of ±25 MPa. Results were sound and in correlation with both convenient destructive methods (cutting and sectioning, hole drilling) and non-destructive method (X-ray diffraction) [10].

Mandal et al. studied on API X-70 steel semicircular pipe section with diameter of 610 mm and 9 mm wall thickness. They concluded that MBN could be used to evaluate stress distribution and could become a nondestructive tool to stand for high-resolution neutron diffraction or photo-elasticity methods [19].

Saquet et al. examined the relationship between BN and the crystalline microstructure, the characteristics of MBN data acquired for more complex microstructures. They were concluded that ferrite matrix with intragranular cementite precipitates increases MBN peak height. On the other hand martensite had low amplitude and a high frequency range [20].

Anglada-Rivera et al. studied on the effect of the applied tensile stress and grain size on MBN and hysteresis loops. They resulted that as applied stress increases, peak amplitude of the Barkhausen voltage also increases. After that the amplitude reached its peak, it begins to decrease with higher tensile stress values. The peak MBN voltage decreases with respect to grain size, because fine grained materials has bigger domains and domain walls movements compared to coarse grained ones [21].

Calibration procedure is a must for MBN method. Because the given unit from MBN measurement device is magnetic parameter and it is needs to transform into MPa unit. Desvaux et al. determined the surface residual stress on the bearing raceways with MBN method. They were shown that MBN method is applicable to circular geometries in a sound and efficient way [22]. On another study, I. Mészáros used MBN method for residual stress determination on ½Cr½Mo¼V type chemical plant steam pipeline steel with a diameter of 27 mm along 15 meters of the length. Specially designed cylindrical measuring heads fitting into the internal surface were used for acquiring the data [23].

K Sapountzi conducted a study on determination of residual stress with MBN method in the heat-affected zone (HAZ) of ST-37 plain carbon steel welds. For the sake of correlation between the MBN data and the stress profile in the welding, Vickers micro-hardness test was applied. MBN results and micro-hardness declared a monotonic relationship between each other. He also stated that acquired magnetic response in the HAZ and fusion zone is higher compared to base metal zone [24].

H. I. Yelbay studied on evaluation of residual stress on welded P355NL2 and API 5L X-70 steel plates with MBN method. The author used both HAZ based and parent metal based calibration in order to achieve most suitable calibration procedure. The author pointed out that calibration procedure was a serious objective due to different microstructures of HAZ and base metal and also renewed that MBN method is applicable techinique for continuous measurement of residual stress [25].

A study conducted by M. Bruns and T. Nitschke-Pagel was used multi-parameter approach. In this technique linear regression analysis of different micro-magnetic techniques are used in tandem with each other. The calibration results for welded joints revealed that multi-parameter approach needs evaluation of residual stress and

changing microstrucre together. The obtained regression polynomial can be used for various residual stress distributions for only one steel grade [26]. In another study of Nitschke-Pagel, it is stated that, micro-magnetic method represents the alternative way of residual stress determination in ferromagnetic steels and weldments. It was emphasized on the advantages of the method. Transportability of equipment, short exposure times and ability of working under severe environmental conditions are the main advantages. Since obtained data do not give stress state without calibration they do not recommend that method on totally unknown stress conditions [27].

C. Kownacki conducted a survey on residual stress estimation with respect to depth of surface layer by using MBN method. The author correlated MBN results with X-ray measurement and also used same probe (μSCAN 500, manufactured by the American ASTStressTech) which was used in this study for MBN measurements. The author stated that due to X-ray measurement process, electrolytic etching was needed to be applied and this procedure also affects residual stress distribution. And in this study it is also emphasized that even MBN method has ability to measure a depth of 1mm below from the surface. It is still not totally explored that the distribution and intensity of MBN as a result of current techniques [28].

Kolařík et al. studied on the effect of grinding and rolling on residual stresses by using X-Ray diffraction and Barkhausen Noise analysis on material 16MnCrS5+HH. To determine the biaxial state of residual stress, they applied XRD "one-tilt" method. Data acquired form the {211} α-Fe diffraction line profiles with accuracy of ±40 MPa. MBN analyses were performed with Stresstech MicroScan 600-1 magnetoelastic analyzer with a standard sensor S1-138-15-0. They concluded that magnetoelastic parameter (mp) such as remanence (B_r) and permeability (μ) could be used for correlation with residual stress and applicable for industrial control procedure [29].

1.3 Aim of the Study

Joining process of the steel pipeline parts includes welding usually results in residual stress at critical level. Welding is also responsible for distortion which creates undesired shape changes making the final product act as if it is a faulty design. Welding parameters, especially weld pass number are charged with great interests to determine final residual stress state.

The aim of this study is to non-destructively monitor the variation of the surface residual stress as a function of the number of weld passes; and also, investigate the reliability and effectiveness of Magnetic Barkhausen Noise Method for measuring residual stresses in welded steels. It is expected that MBN method for residual stress measurement will create vast of opportunities with its accuracy and continuous measurement ability compared to conventional ones.

CHAPTER 2

THEORY

2.1 Residual Stress in General

Residual Stresses are the remaining stresses after the original source of stress removed from the material. Residual stresses are formed due to the incompatibilities along the various regions of the material. Plastic deformation history, microstructure, time and temperature are the key factors of the final residual stress state of the material (Figure 1) [30]. Lots of material properties play role to evolve the material its final residual stress state. These are thermal properties such as; thermal conductivity and heat capacity, mechanical properties such as; elastic modulus and Poisson's ratio, kinetic and thermodynamic properties such as; kinetics of transformations and phase transformation mechanisms [28].

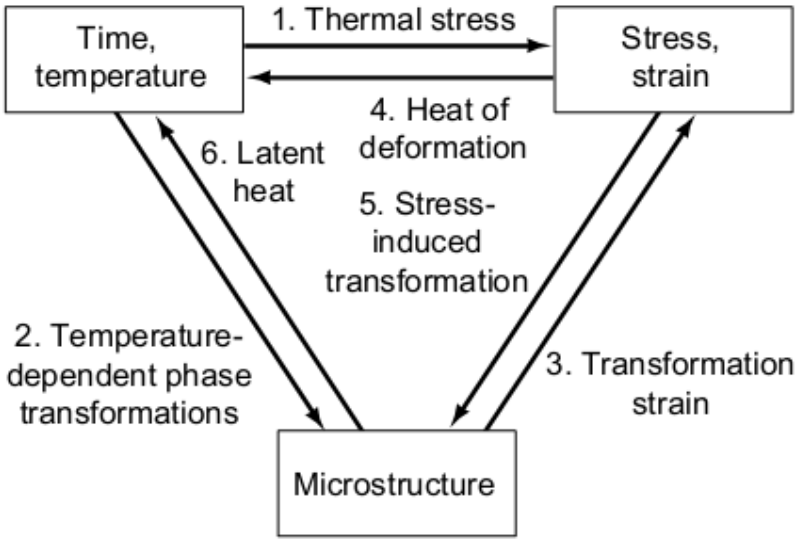

Figure 1: Relationship between the factors that occurs the final residual stress [30]

Importance of Residual Stress must be taken into account for industrial applications in general, because several failure reasons are affected by residual stress. It affects fatigue performance in long or short term. Considering damage tolerant design, crack initiation and propagation are related deeply to residual stress. Distortion is also another parameter related to residual stress resulting in after welding operation. Even stress corrosion cracking (SCC) and hydrogen initiated cracking (HIC) are related to residual stress on the body.

Residual stresses must carefully be measured and monitored. Processing parameters must be optimized in order to avoid undesired residual stresses. It provides useful data for fatigue life of the body to reduce catastrophic failures. It also confirms the situation that repairing procedures are done in true manner.

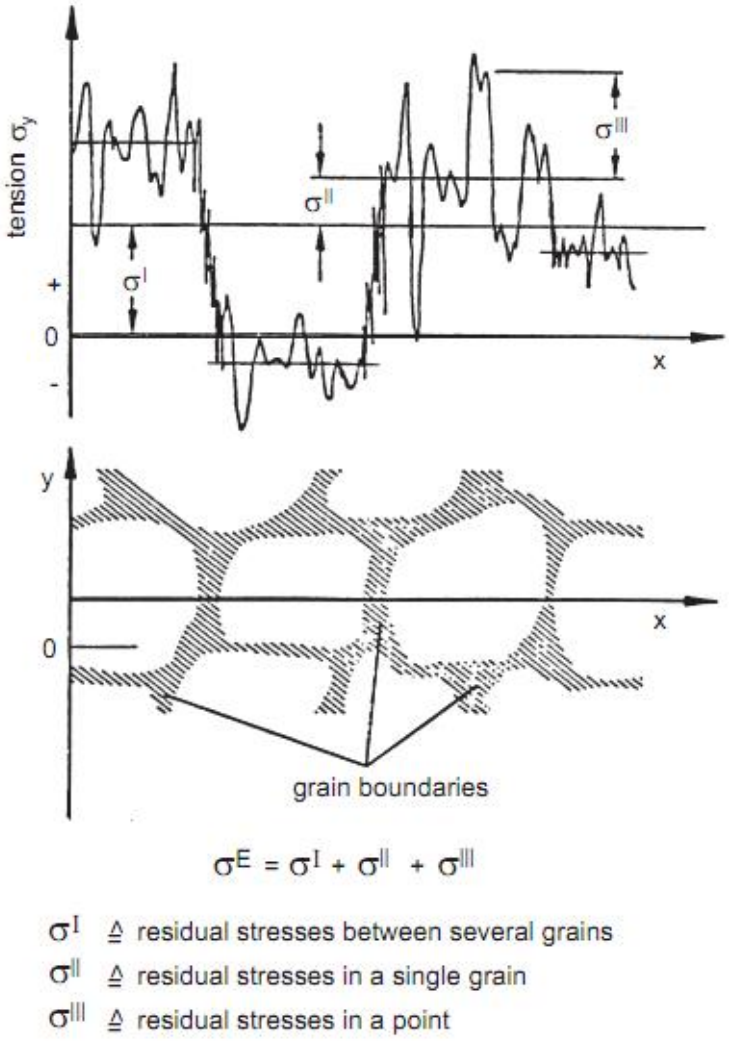

Figure 2: Typical distribution of residual stresses [7]

Residual stresses are categorized into three types according to the form in which it exists as seen on Figure 2. Type 1 residual stresses can be termed as macrostresses. They are of continuous form on the material surface neglecting the microstructure of the material itself. These type 1 residual stresses are commonly results in plastic deformation during primary or secondary procedures of production. Type 2 residual stresses can be termed as intergranular stresses. Type 2 residual stresses are in scale of a few grain diameters and residual stresses are results in inhomogeneity at the grain level. Type 2 intergranular stresses are generally originated from variations at the slip behavior of the material. The final and finest of all, Type 3 residual stresses can be termed as microstresses originate from the variations of the material in an atomic scale. They are commonly dislocations and point defects. These types of residual stress are exists in their scales however they can be in tandem with each other and can be aggregated in order to change the total residual stress from microscopic to macroscopic level [30].

Residual stress must be balanced to zero for the body. Tensile residual stress must be compromised with the compressive residual stress in order to keep the equilibrium. Residual stress statute through the body needs to satisfy Equation 1 where A represents the area that stress balance needed to done [31].

$$\int_A \sigma ij dA = 0 \qquad 1$$

Residual stress can occur on the surface and at the sub-surface of the body. In general, surface stresses affect sub-surface crack as there exists a sub-surface defect. Fatigue cracks generally initiate from the surface of the body. So determination of crack initiation and propagation has a detrimental role during non-destruction evolution procedure. To fully cover the consequences of primary and secondary procedures done on the body, nature of the surface and sub-surface stress gradients must be examined in a careful manner.

Residual Stress may have different sources; at production stage, due to the wear during service time and just from the material itself. Plastic deformation, thermal origins and phase transformation are the main source of residual stress.

Temperature gradients along the material itself introduce thermal misfit stresses. Fast cooling rate is the most common example of it which forms tensile stresses on the outer surface and compressive stresses at the interior of the material. If there are sharp thermal gradient changes along the body of the material, possible plastic deformation can be formed on the body in a non-homogenously nature. Thermal misfits in intergranular stage resulting in Type 2 residual stress also exist. It does not matter whether the body is multiphase or single phase because; even at the single crystal stage thermal expansion occurs in an anisotropic nature [7].

Phase transformations also affect the residual stress state. Sudden distortions along the crystal lattice cause misfit between transformed and untransformed regions. This results in residual stress along the body with distortions noticeable in macro level. In steels martensitic transformation is a very distinctive example of these kind of residuals stress formation. Nucleation of martensite occurs with a twinned structure to minimize strain energy also that the residual stress [7].

During welding thermal gradient is the main residual stress source for this joining procedure. As a result of the characteristics of welding, non-uniform plastic deformation is introduced to body. Weld metal and base metal interaction has significant importance due to the plastic strain introduced by local thermal gradient. These plastic strains, occurred as a result of welding, are the reason for residual stress in the weld metal and in the base metal in conduction with weld. Residual stress, shrinkage and distortion are formed when the weldment returns to initial temperature state. Temperature and residual stress creation is explained in Figure 3. Plate shown in Figure 3 is welded along the X-axis with speed of ν, initiating from point O on the cross-section of X and Y axis. Figure 3-a shows the welded region in which plastic deformation is happened. Figure 3-b and c shows the temperature change and stress change respectively.

Through A-A line, there is no temperature and thermal stress variation because of the thermal gradient as a result of welding in negligible. The distance between arc and A-A line is the main factor to satisfy that result.

Through B-B line, in which the welding arc initiates, temperature close to arc is dramatically high compared to other regions away from the arc along Y-axis. Stress

is almost zero under the weld arc through B-B line because of the fact that material cannot carry load under that non-solid state. Compressive stress is produced close to the arc as a result of surrounding material which restrains the thermal expansion of the volume is in dramatically low temperature state compared to weld metal. while moving away from the weld metal, temperature decreases and compressive stress reaches its maximum. After these compressive regions, tensile stress is introduced to balance total stress of the region.

Through C-C line, temperature close to arc is decreasing as it gets away from the arc initiation point; however temperature away from the arc is increasing compared to B-B line. This is because of the total heat input to the material increasing as the welding procedure continues. Temperature difference between weld metal and base metal is much softer here along C-C line compared to B-B line. Tensile stress region near the weld is occurred because weld metal and base metal cools down together and cause shrinkage. Tensile stress along weld line, compressive stress region is formed through C-C line also tensile stress is formed in order to balance the total stress.

Through D-D line, temperature gradient between weld and base metal is nearly vanished. So temperature change is negligible. Tensile stresses with increased in value compared to other lines are formed along weld and compressive stresses are occurred to counter the stress balance of the region [32].

Residual stresses, local shrinkage and distortion are resulted from that thermal gradient. At the steel weldments, highest amount of residual stress is expected through the length of the weld in the weld metal and HAZ [7]. Through the parts of the HAZ where the temperature exceeds the critical values for phase transformations, transformation-induced residual stresses occur. As the effect of phase transformations is dominant compressive residual stresses are formed in the transformed areas [33].

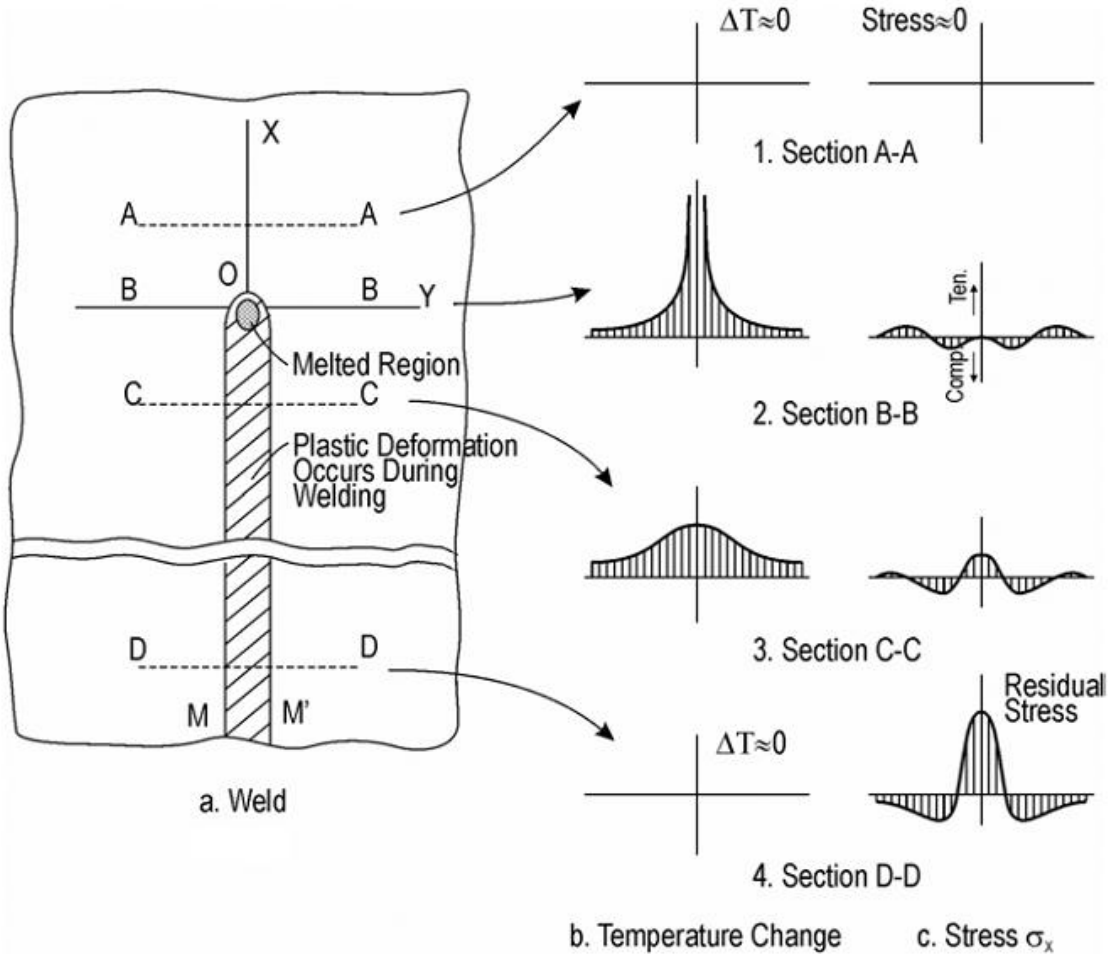

Figure 3: Representative graph of longitudinal thermal residual stresses and temperature variations during welding procedure [7]

Thermal stresses formed due to temperature gradient are not the only factor affecting residual stress during welding, melting and solidification must be taken into account considering the fusion line. Metallurgical transformations are also responsible for the amount of the tensile and compressive stresses. In general at weld metal, expansion is introduced as a result of martensite formation reducing the tensile stresses near the weld line. Metal movement is another to consider during welding. Since at first pass each material is free to move and during further weld passes, body is not allowed to move. This metal movement can even form minor residual stress compared to other factors. In this study no butt weld is done so, this phenomenon can be considered as negligible [32].

Residual stresses as a result of welding procedure are divided into two categories. These are the residual stresses formed after welding of the strain-free body and

reaction stresses that are formed due welding of body with a restraining agent. Figure 4 shows longitudinal and transverse residual stresses distribution in a butt welded body.

There in Figure 4, σ_x refers to the stress distribution through the y-axis, parallel to the welding and σ_y refers to the stress distribution through the x-axis, transverse to the welding. As noticed from the Figure 4-b, regions with high in tensile stress are placed close to weld and compressive stress regions are followed them. This kind of residual stress distribution happened because maximum residual stress, σ_{max} is obtained at weld zone and tension stress region with thickness of b takes place. Maximum residual stress, σ_{max} can be close to the yield strength value of the material considering low carbon steel weldments.

Figure 4-c shows the transverse residual stress distribution along X-axis. Considering the curve 1, tensile stresses are formed in the mid part of the plate and compressive stresses are formed at the finishing regions of the plate. When an external restraint is introduced to the system like clamps holding the weldment, reaction tensile stresses are added to the system in a uniform level as shown in curve 2. Actually multi-pass welding procedure is responsible this phenomena just by itself. For welding operations including plate with thickness over than 25mm with multi-pass welding, first pass became the source of reaction tensile stress and make external restrained has negligible effect on the final residual stress statue [32].

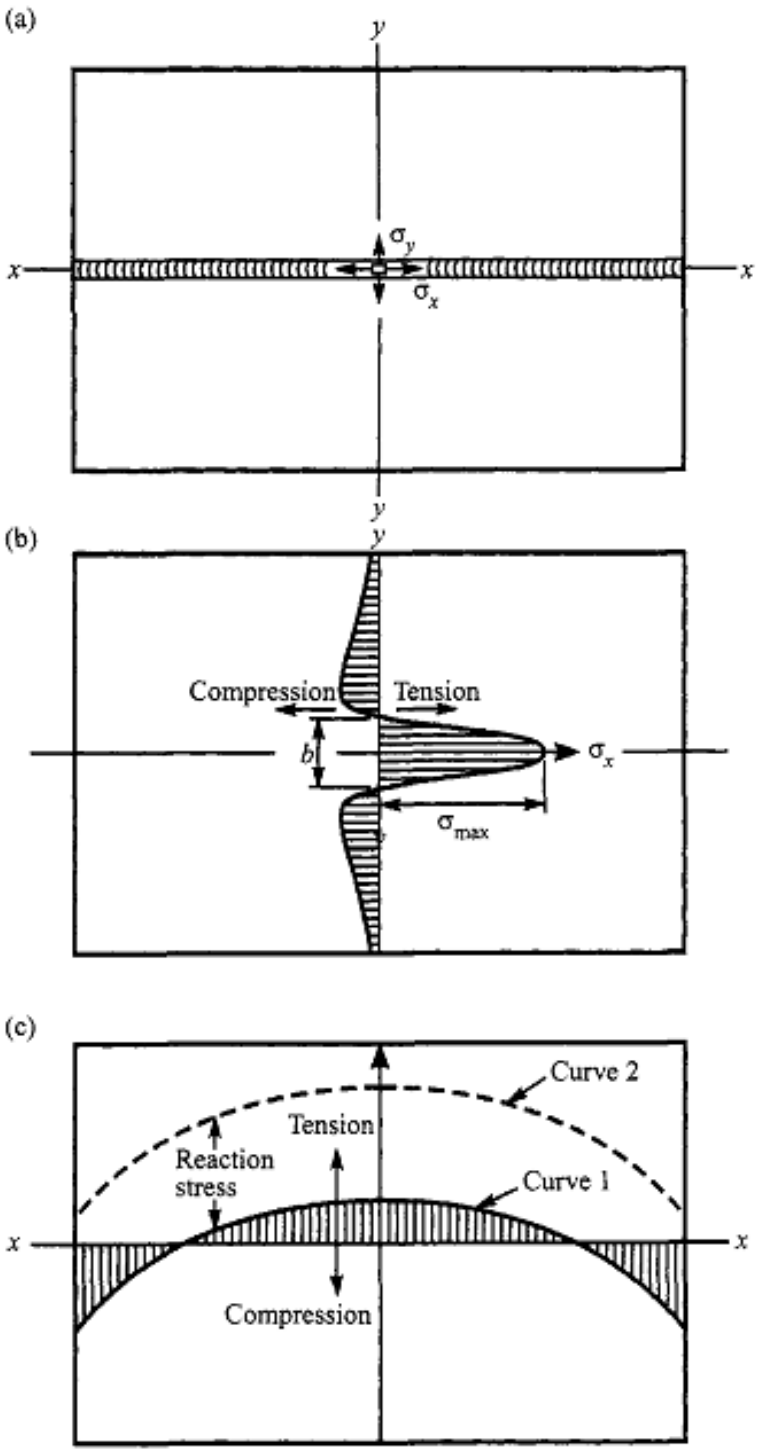

Figure 4 : (a) Residual stresses distribution in a butt welded steel plates (b) σ_x distribution through the y-axis (c) σ_y distribution through the x-axis [32]

2.2 Distortion in Weldments

Different type of distortion is introduced as a result of different types of joints as welding procedure takes place. Various type of shrinkage occurs during welding procedure including transverse shrinkage which is perpendicular to the weld line, longitudinal shrinkage which is in parallel with the weld line and angular distortion in which the body rotates around the weld line.

Figure 5 shows representational view of dimensional changes during welding procedure. Transverse shrinkage is shown on Figure 5-a. during this type of distortion each part is in free to move situation. Transverse shrinkage is considerably higher in butt welds compared to fillet weld since in the fillet weld bottom plate remains in solid state during welding.

Longitudinal shrinkage is shown on Figure 5-b. As it goes further away from the intersection of weld and base metal, amount of longitudinal shrinkage gets larger. Angular distortion is seen on Figure 5-c. Distortion is caused by the non-uniform transverse shrinkage along in the direction of the thickness. Angular distortion can be minimized with controlling the numbers of weld passes from and bottom of the plate.

Angular distortion of a fillet welds is seen on Figure 5-d. It is resulted from the improper balanced shrinkage of the plate from each side.

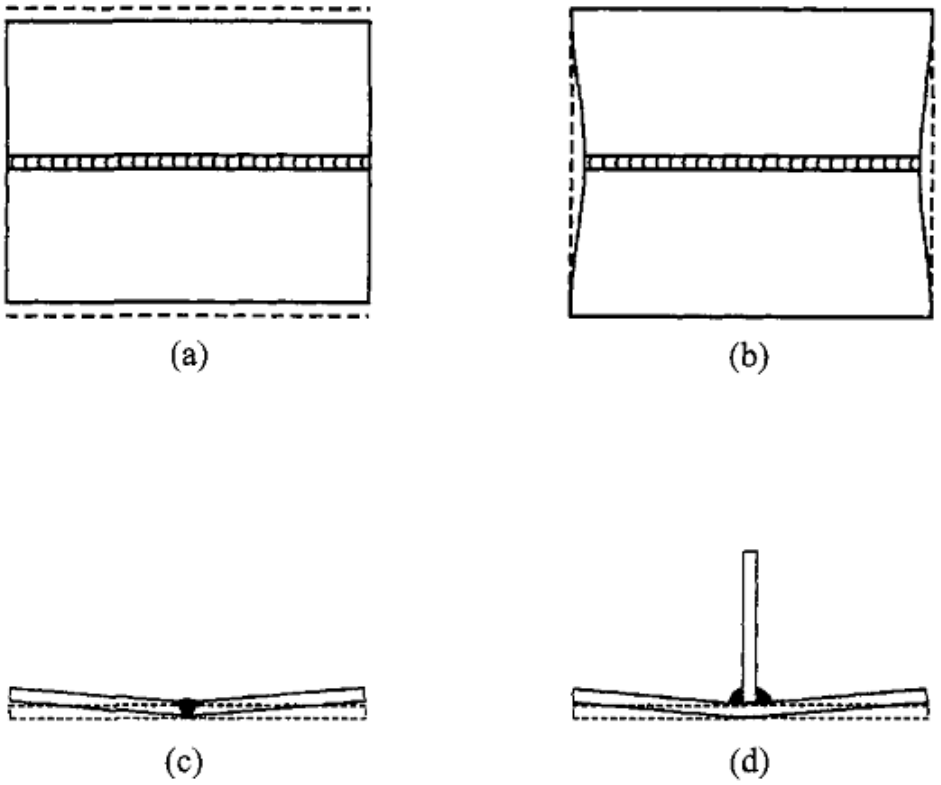

Figure 5: Representational view of dimensional changes during welding procedure: (a) transverse shrinkage, (b) longitudinal shrinkage, (c) angular distortion, (d) angular distortion of a fillet welds [32]

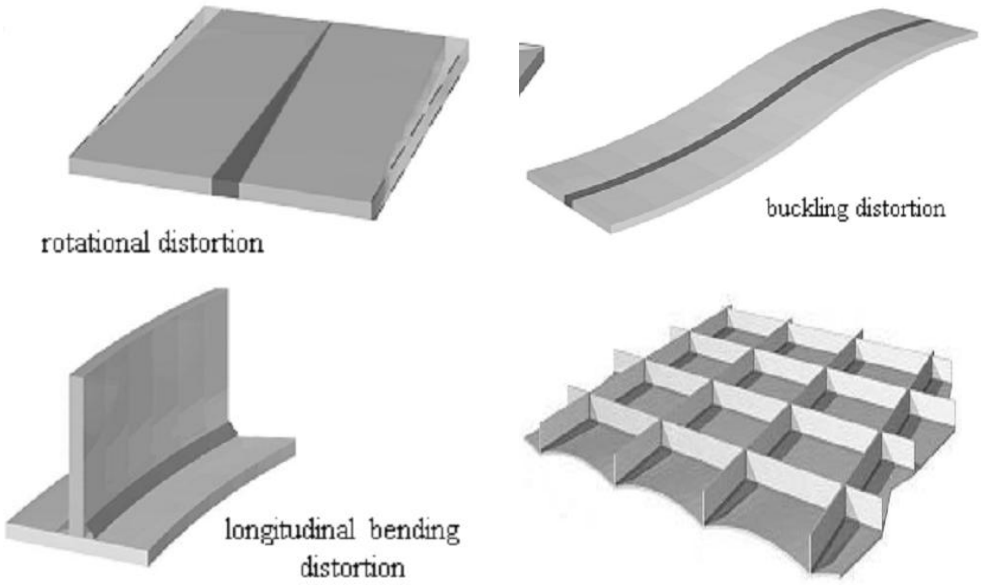

Figure 6: Schematic representation of several types of weld distortion [34]

Relatively simple problems are enlightened in Figure 5. On the other hand industrial distortion problems are much more complex. In Figure 6, schematic representations of several types of weld distortion are given.

Rotational distortion usually exist while butt welding of two parallel plates. Main reason of this type of distortion is the welding of the total weld distance continuously. During welding transverse shrinkage occurs. As weld beam moves from welded section to the non-welded section, non-welded portion of the body cause rotational distortion.

Longitudinal bending distortion happens during the production of long beam weldments. Mismatch between desired weld axis and application weld line allows to formation of bending moments with the longitudinal shrinkage of the weld metal.

Buckling distortion usually happens during thin plate welding. Regions away from the weld having compressive residual stresses are responsible for this defect. To avoid buckling distortion body must be kept in a rigid state in order to restrain the movement of the body perpendicular to the weld line. Buckling distortion may occur even if the restrainers of the body are removed. Panel length, thickness and heat input values are critical factors to be examined carefully in order not to have this kind of distortion.

Bottom plate is fillet welded with longitudinal and transverse frames. Main source of bending distortion of the bottom plate of a welded panel structure is that every fillet weld at the panel has angular changes that deform the bottom plate. Buckling strength of the bottom plate is lowered by the initial distortion when compressive loads are applied to the bottom plate. This welded panel structures are applied to the heavier constructions such as ships and bridges so this kind of distortion must be kept in minimum level [32].

2.3 Residual Stress Measurements by Magnetic Barkhausen Method

Residual Stress measurement methods could be examined as destructive (sectioning, hole drilling, contour method) and non-destructive methods (X-ray diffraction, ultrasonic, micro-magnetic methods). Destructive methods are also called

mechanical methods examine the variations in distortion of the component. It can be done in two steps; first residual stress is generated and measured second, material is removed to make material relaxation the stresses [35]. Considering non-destructive methods, material properties related to stress, are measured. Magnetic Barkhausen Noise (MBN) is a challenging method for residual stress measurement.

Pierre-Ernest Weiss predicted existence of the ferromagnetic domain wall structure in 1907 [36]. German physicist Heinrich Barkhausen in 1919 reveals the secret behind discontinuous character of the movement of magnetic domain walls [37]. Domain is the region of uniform magnetization where it is uniformly magnetized along an easy axis and it has zero exchange energy and the anisotropy energy. Magnetization of every domain in the body is at the saturation level. Vector sum of the magnetization along all domains is the net magnetization of the body. Considering an infinite medium which is non-uniformly magnetized, it needed to be sectioned into regions where uniformly magnetized domains exist. Since, in natural state domain alignment occurs randomly, transition layers are needed to separate these domains. These transition layers, domain walls, are responsible for realigning the magnetic moments between the domains. They do not belong to any domain itself and have finite thickness [22].

Discontinuous character of the magnetic domain walls resulted from the imperfections in the crystalline structure, such as dislocations, grain boundaries, precipitates and vacancies. The domain wall movement stops suddenly when the defect is encountered. It stays remained until field reaches the threshold value. When the applied field overpasses the threshold value the domain wall movement continues up till the next defect. The existing interaction energy between the defect and the domain wall determines the blocking capacity of the crystalline defect. When it is viewed together, these sudden domain wall movements results in Magnetic Barkhausen Noise (MBN). This abrupt domain movement, discontinuous increments are called Barkhausen jumps (Figure 6).

Actually these discontinuous increments, Barkhausen jumps, are voltage spikes. In the beginning it was stated that these discontinuous increments were resulted from the sudden rotation of single domain however it is now revealed that discontinuous domain wall motion is the key parameter affecting for the discontinuities in

magnetization. MBN is formed as result of both sudden rotation of single domain and discontinuous domain wall motion [38].

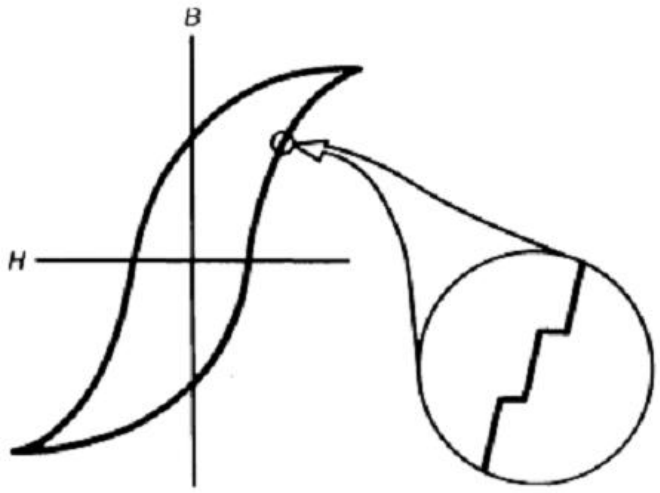

Figure 6: Hysteresis loop as a result of Barkhausen jumps [39]

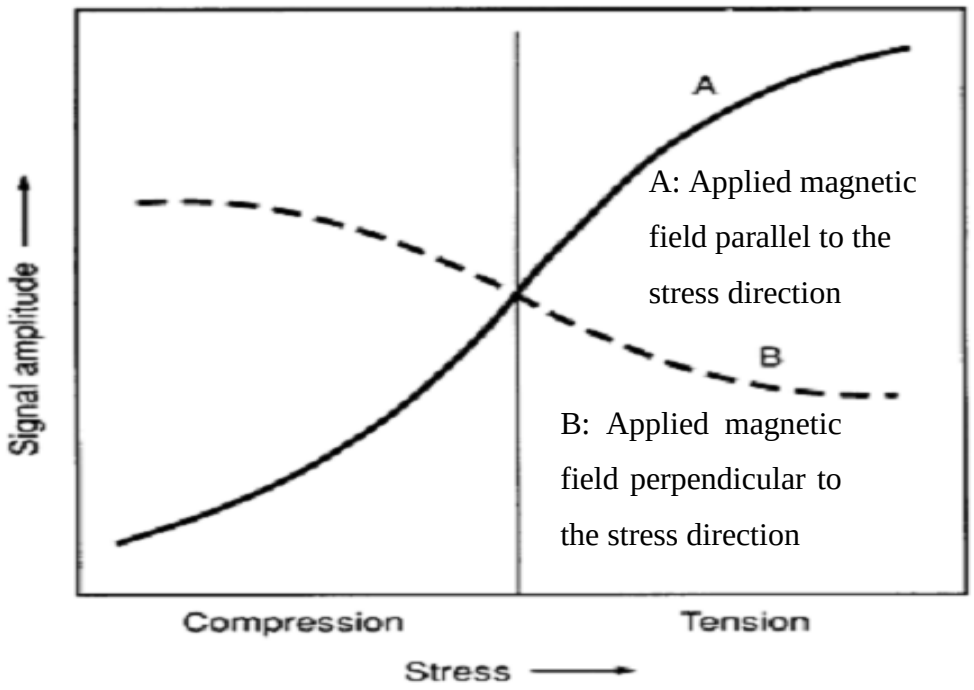

Figure 7: Applied stress dependence of MBN signal amplitude with respect to the applied magnetic field [39]

The defects in the crystal structure are responsible for the blocking of the Weiss domain walls so MBN method is sensitive to changes in the magnetic microstructure as a result of the metallurgical microstructure of the material itself. In the remaining applied magnetic field, domains which have magnetization parallel to the applied field increase the magnetic field and domains having magnetization perpendicular to the applied field decrease the magnetic field up till it diminishes [37]. Considering the magnetization of a ferromagnetic material, it usually results in change of physical dimension. These dimensional changes (longitudinal, transverse, or volumetric) are called magnetostriction. Figure 7 represents materials having positive magnetostriction coefficient on the other hand for materials with a negative magnetostriction, MBN amplitude has the opposite altitude.

There exist two ways for the domain to move. In first way it rotates in a coherent way to a direction parallel to the applied field with the help of magnetization and in second way domain wall moves at the expense of change in total magnetization state which localized at the domain boundary. In Figure 8 domain wall movement with respect to magnetic field is shown. In natural state at zero magnetic field domain walls rest as stationary. Domain walls start to stretch at lower applied magnetic field (H) and they are able to return to its non-magnetized state when applied magnetic field diminished. As long as it returns to original state when magnetic field diminishes, it is called reversible motion. In irreversible domain wall movement, as the applied magnetic field increased to a level in which the growth of domains occur. By this domain growth, domains are aligned nearly parallel to the applied field and grow at the cost of non-parallel aligned ones. After that point it further continues until single domain aligned to the direction of one of the easy axis. As applied field increases domain rotation procedure is the dominant one and work against the anisotropy forces. As it further reaches saturation with dramatic increase in the applied field relatively small increase occurs in magnetization [40].

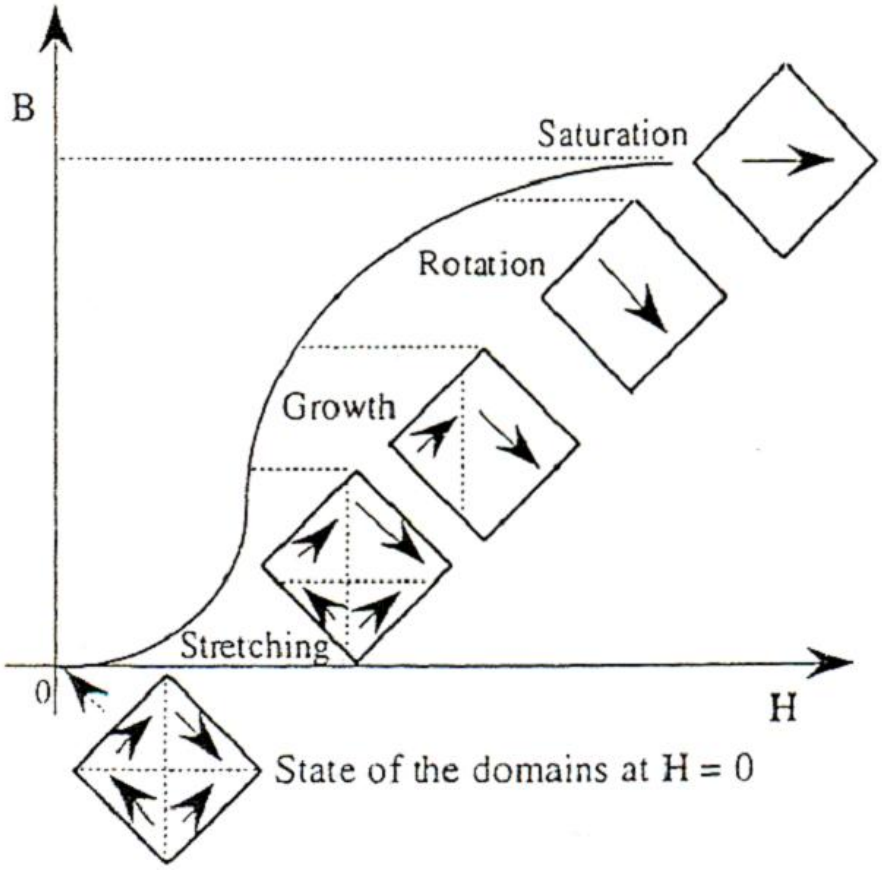

Figure 8: Magnetization state change with the applied magnetic field [41]

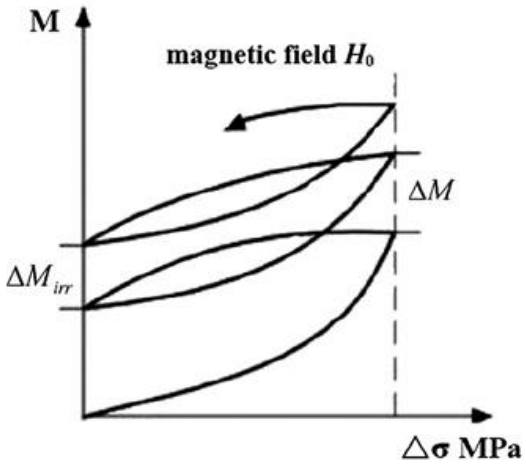

Figure 9 Schematic representation of relationship between cyclic stress and the magnetization of ferromagnetic materials [42]

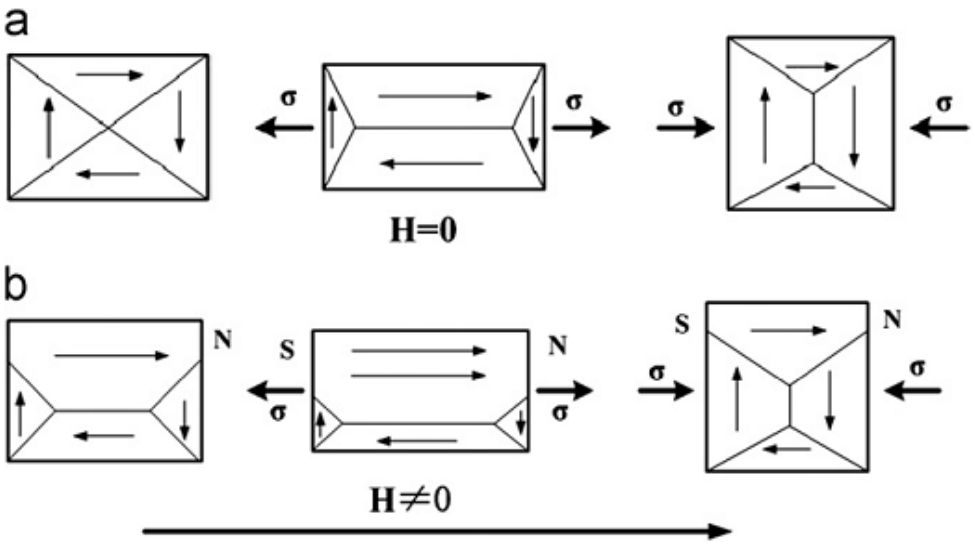

Figure 10 Movement of magnetic domain walls under the influence of applied stress [42]

Applied stress has effect on the magnetic properties of ferromagnetic materials. *Permeability* (the degree of which the material can be magnetized, μ), *coercivity* (the magnetic field needed to reduce the magnetization from an arbitrary level to zero, H_c) and *remanence* (the remaining induction or magnetization as the field has been removed after the material has been magnetized to saturation) of ferromagnetic materials are affected by the elastic stress. Total magnetization (M) of the material consists of two components; reversible component, M_{re}, and irreversible component, M_{irr}. As a result of mechanical stress, domains have to pass through these pinning sites. As this event occurs for every loading cycle, difference of irreversible magnetization (ΔM_{irr}) is formed (Figure 9) [42].

Applied stress also affects the domain wall movement. There exists no magnetization in macro scale and the magnetic moments have random distribution in a ferromagnetic material. Consider that the material has applied tensile stress. Domains having magnetization in parallel with the applied tensile stress increase at the cost of the non-parallel domains and restrain the total volume. And same thing is also valid for the compressive stress. Domains having magnetization in perpendicular to the applied compressive stress increase and restrain the total volume too [37]. The magnetization in situation with no defect is shown in Figure 10-a and magnetization

under the influence of magnetic field (H) in situation of corrupt wall is shown in Figure 10-b.

MBN value is sensitive to changes in both applied stress and the magnetic field. If the stress and magnetic field enhance the domain wall movement, measured MBN level increases. If the stress and magnetic field inhibit the domain wall movement, measured MBN level decreases [41] [43].

Defects in the crystal structure like dislocations, impurities results in an energy lost during magnetization process. These defects cause the hysteresis formation. Hysteresis loop obtained by MBN measurement becomes narrow when applied stress is parallel with the remaining magnetic field and becomes wider when applied stress is perpendicular to the field with smaller amount in amplitude [44]. Not only is the hysteresis loop affected by applied stress, but also it is affected by the hardness of the material. Generally it is difficult to magnetize mechanically harder materials (Figure 11). Softer material's hysteresis loop with higher flux density (B), acquired at large magnetic field (H) value is larger than the harder material [45].

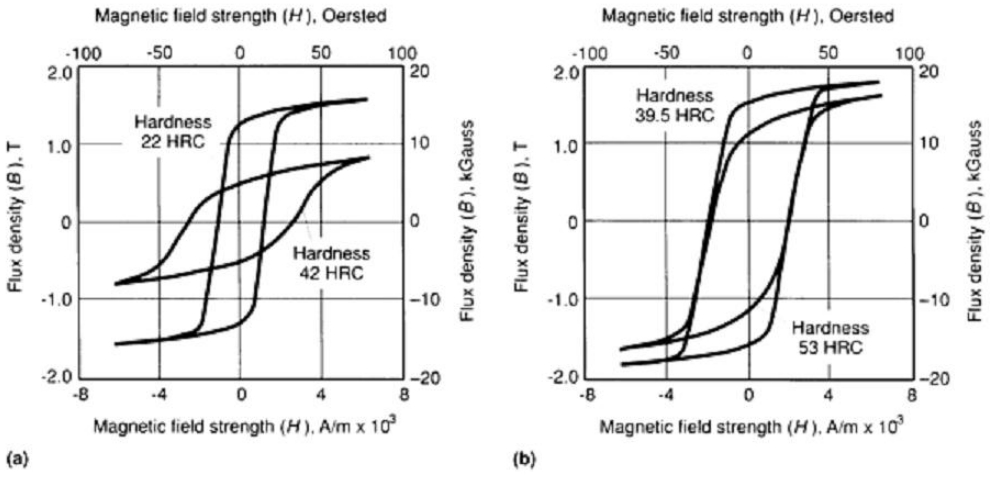

Figure 11: Hysteresis loop and mechanical hardness relationship (a) AISI 410 stainless steel (b) SAE 4340 steel [39]

Set-up for MBN measurement in basic includes signal generator with power amplifier, biasing magnet with an inductive search coil in it and a display record device for data storage. Time-varying magnetic field is applied to the specimen by a C-shaped electromagnet. The inductive coil sitting on the specimen acquires the magnetic field changes as a result of the abrupt movements of the magnetic domains.

Acquired signal is in form of burst of noise like pulses (Figure 12). Stress state of the specimen is clarified with the distinct properties of the signal (Figure 13). These properties are the applied magnetic field strength where the maximum amplitude happens and root mean square (RMS) or the maximum amplitude of the BN burst [39]. The statistical measure of the magnitude of a varying quantity is called the root mean square (RMS) and is calculated using Equation 2 [46].

$$MBNrms = \sqrt{\frac{\sum_{i=1}^{n} Vi - Vm}{n-1}} \qquad 2$$

where:

V_i = voltage value measured for the i^{th} observation;

V_m = average signal value;

n = number of signal observations

Envelope features of the signal are also gathered from the analytical signal of the MBN signal. Generally two parameters, peak amplitude (MBN_{apeak}) and Peak position (MBN_{ppeak}) are obtained. MBN_{apeak} is the maximum value of the envelope amplitude and MBN_{ppeak} is the location of the peak position as seen on Figure 13.

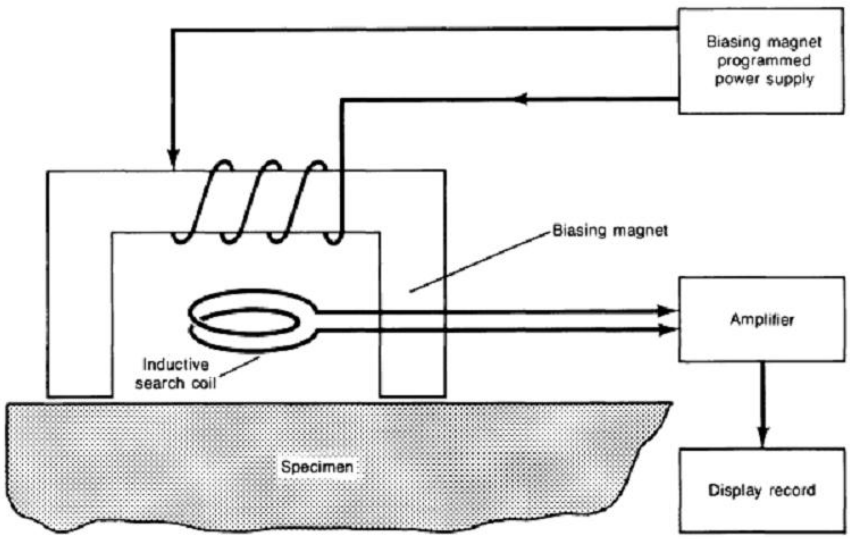

Figure 12: Setup for MBN measurement [39]

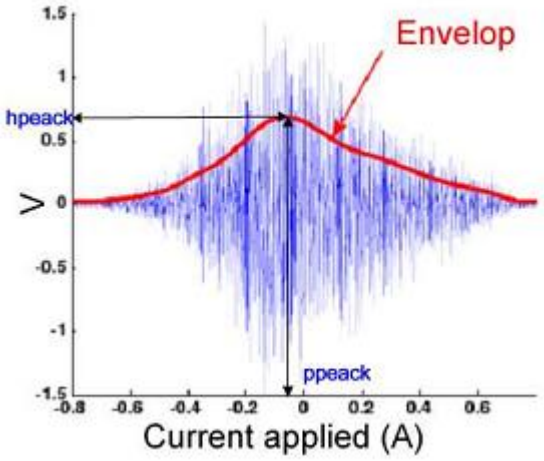

Figure 13: An example of MBN Signal envelope [46]

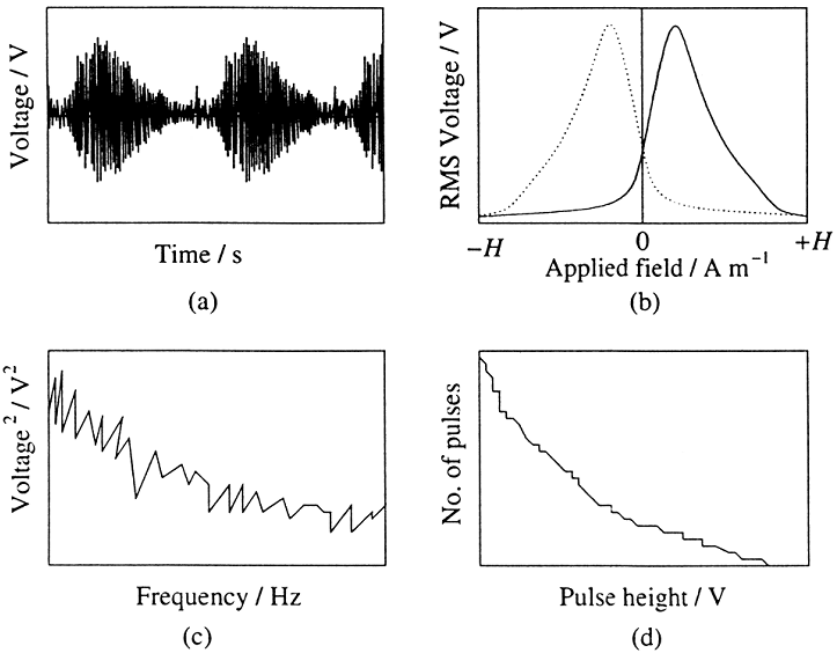

Figure 14: Various characterization plots obtained from raw MBN data [47]

Raw data obtained from MBN measurement includes voltage pulses and related applied magnetic field strength values as a function of time. It is amplified and filtered in order to obtain the following parameters for the purpose of material characterization. From MBN measurement obtained raw data gives information about; MBN profile (fingerprint), amplitude (frequency) spectrum, pulse height distribution and B-H curves (simulated hysteresis).

In this study MBN profile (fingerprint) is the main parameter that is used for characterization of the weldments. MBN fingerprint is the plot of local RMS value and applied magnetic field strength with a determined sampling frequency. Various field cycles which is determined by the number of burst, is associated with instant RMS values to plot a MBN fingerprint. MBN peak height and magnetic field strength are the parameter, used for material characterization, obtained from MBN fingerprint plot. Amplitude (frequency) spectrum is the plot of square power of voltage and frequency. Fourier analysis is used in order to obtain the frequency content used for amplitude spectrum. Pulse height distribution is the plot of number of pulses against the voltage value. It consists of size distribution of pulses. B-H curves (simulated hysteresis) obtained by accumulating the sum integral of rectified bursts. Since simulated hysteresis is obtained by local saturated magnetic state, it cannot be classified as true value for the whole body of the specimen. On the other hand coercivity, remanence and permeability can be determined from that simulated hysteresis [47].

CHAPTER 3

EXPERIMENTAL PROCEDURE

The first part of the experimental procedure includes determination of residual stress as a function of weld on clamped API 5L X-70 steel plates via magnetic Barkhausen noise method (MBN). Second part includes determining the amount of angular deflection and residual stress again as a function of weld passes on non-clamped steel plates.

3.1 Heat Treatment

Six API 5L X-70 grade pipeline steel plates were used. The chemical composition is given in Table 1, which satisfies the API Specifications [1]. The CCT diagram for nearest average chemical composition is given in Figure 15 [3].

Table 1: Chemical composition (wt. %) of API 5L X-70

C	Si	Mn	P	S	Cr	Ni	Cu	Nb	Ti	V	Al
0.065	0.258	1.66	0.009	0.003	0.151	0.037	0.049	0.051	0.010	0.0525	0.017

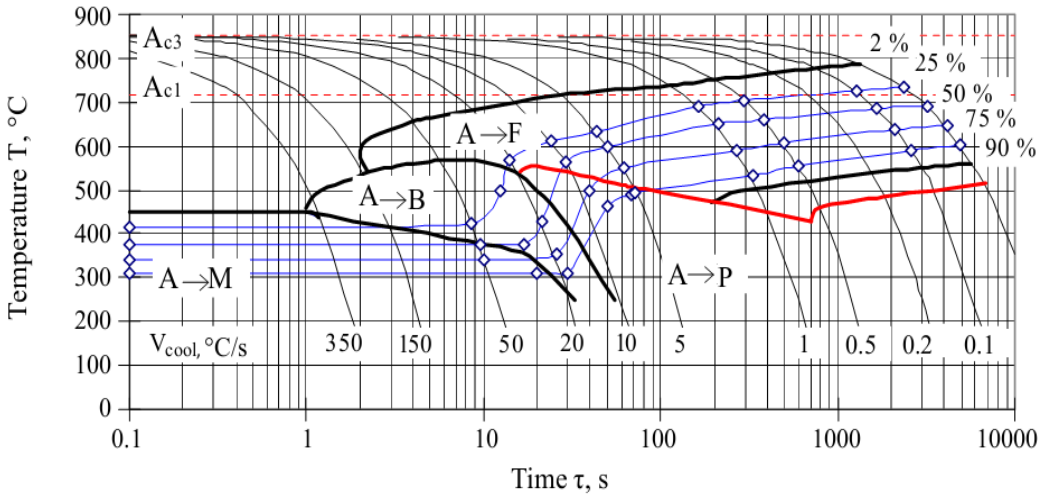

Figure 15: CCT diagram for API 5L X-70 adopted from nearest average chemical composition [3]

As a result of controlled rolling in the production route of API 5L X-70, directionality is introduced to grains of the sample. This directionality in the grain orientation results in differences during residual stress measurement. Due to the formed texture residual stress statue is different for rolling (longitudinal) and transverse direction. The difference between the rolling and transverse direction is nearly doubled at the received state of the material.

Heat treatment procedure was applied in order to reduce the magnetoelastic parameter (MP) difference between rolling and transverse direction, because longitudinal residual stress was measured during experiment. At first, stress relief treatment was applied at 620 ^{0}C for 2 hour. Unstable data still obtained and directionality yet not fixed. Finally annealing procedure was decided to be done to minimize directional response. In figure 16, magnetoelastic parameters (MP) of the as-received, stress relieved (620 ^{0}C / 2h), and normalized (960 ^{0}C / 1.5h) samples are shown.

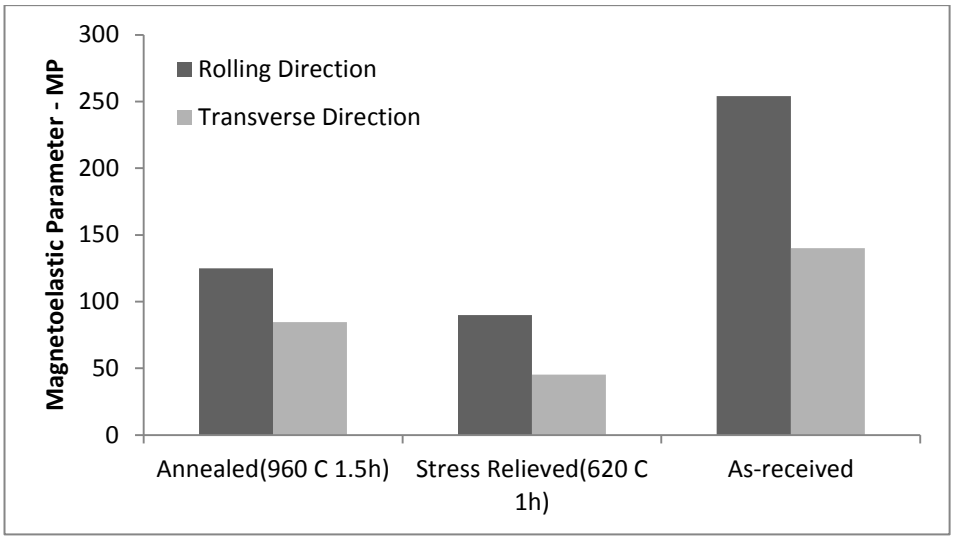

Figure 16: Configuration of the MP results in the rolling direction and transverse direction at normalized, stress relieved and as-received state

3.2 Preparation of Test Samples

Six API 5L X-70 steel plates with initial thickness of 19.6 mm were used. Each specimen was cut and machined to dimensions of 280x150x18mm. Prior to machining operations, heat treatment was applied to minimize the directionality of the measurements. During heat treatment because of the equipment used, decarburization of the samples was inevitable. To get rid of decarburized layer on the surface samples were grinded. To avoid differences in dimension, all six specimen were set at the same time on the stoning bench, to avoid grinding burn oil-water cooling is applied at the stoning bench and finally to avoid changing residual stress state during grinding all samples were grinded same amount from front and back sides.

After grinding procedure, V-shaped weld grove was chosen because of the steel grade and welding electrode. V-shaped grooves were machined with a width of 18 mm and depth of 9 mm through the width, in the middle of each plate. Figure 17 shows the machining steps of the plates and the final dimensions of the specimen is given in Figure 18.

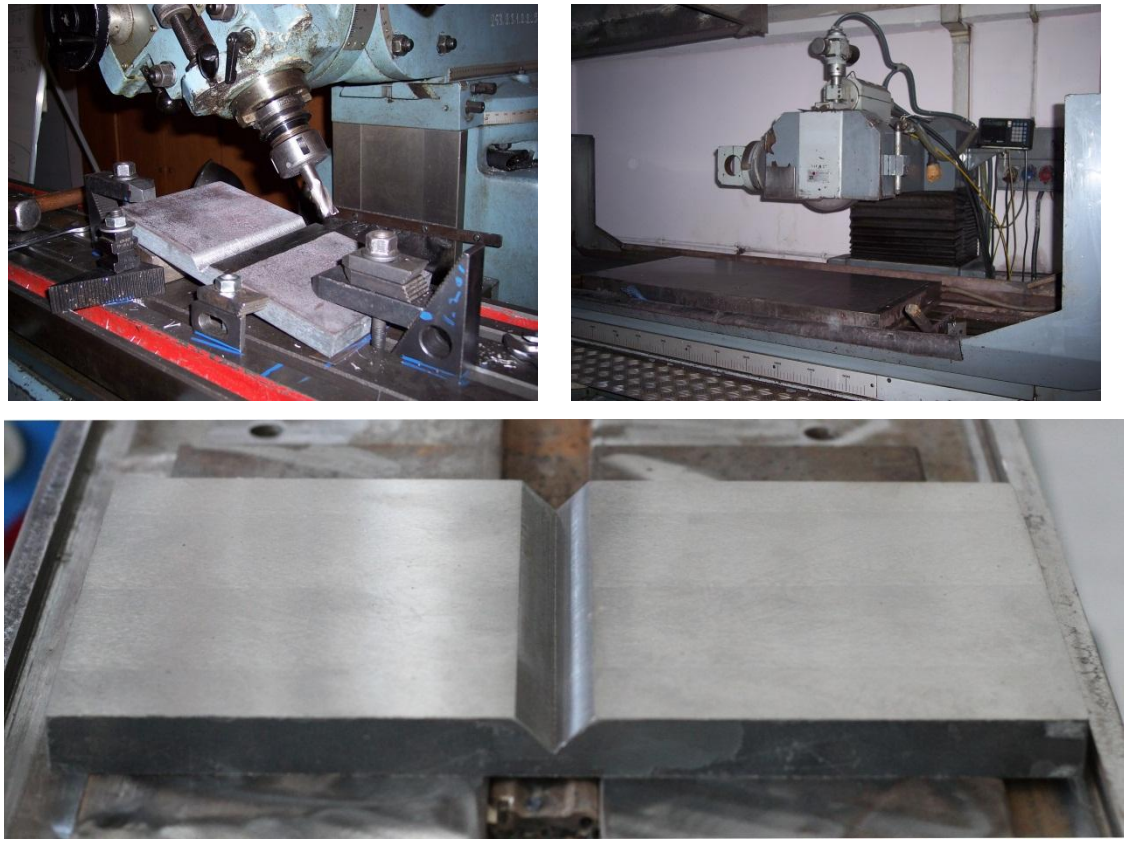

Figure 17: Machining of V-grooved plates

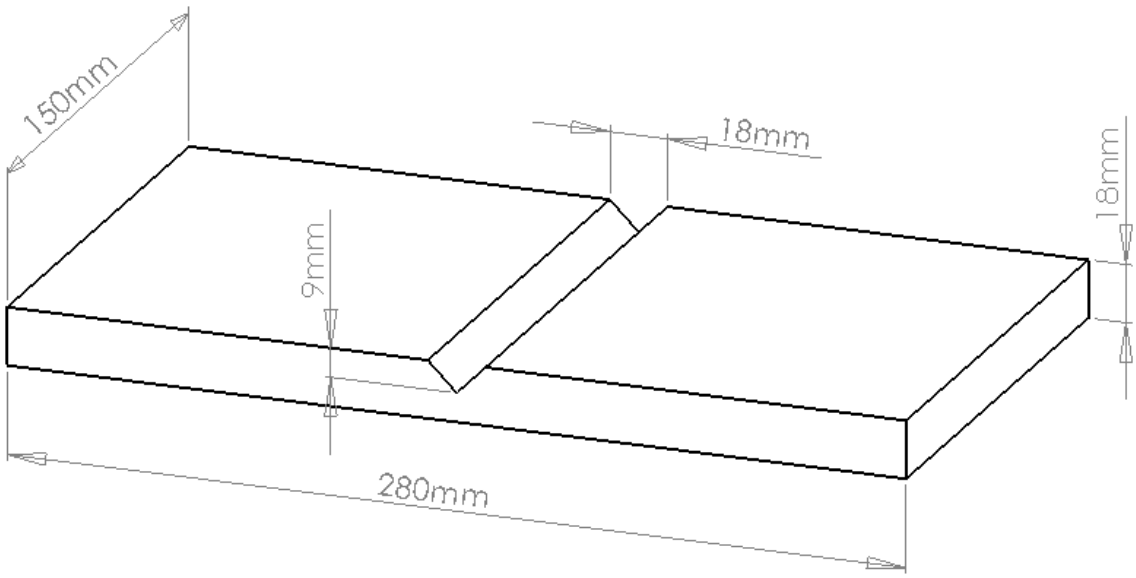

Figure 18: Final dimensions of the API 5L X70 steel plates

3.3 Determination of Welding Parameters and Welding Operations

Three API 5L X-70 plates were used for residual stress measurements and another three plates were used for deflection measurements. Each set was subjected to 2, 4 and 8 weld passes with the same welding parameters. Heat input and line energy values (Table 2) calculated with Equation 3 and Equation 4;

$$E = (A \times V) / \vartheta \quad (3)$$

$$H = E \times \text{weld pass\#} \quad (4)$$

E: Line Energy, A: Ampere, V: Voltage, ϑ: Welding Velocity, H: Heat Input,

WFS: Weld feeder speed, LWS: Linear Welding Speed

Table 2: Weld Parameters

weld	# passes	WFS (m/min)	U (V)	I (A)	LWS (cm/min)	E / pass (kJ/mm)	Efficiency	H (kJ/cm)
A	2	11.5	29	290	400	1.26	0.8	20.2
B	4	9	25	230	600	0.58	0.8	18.4
C	8	6.5	21	170	800	0.27	0.8	17.1

The parameters that affect residual stress were chosen as the number of weld passes and heat input. Heat input values are chosen as it was in Table 2, considering the 18mm thickness of the steel plates used. The plates were fixed with 4 clamps from each corner to inhibit deflection during welding.

During welding operations ISO 14341-A G 42 3m G3Si1 electrode with diameter of 1.2mm was used. Shielding gas for welding procedure consists of 20% CO_2 and 80% Ar. Chemical properties and mechanical properties of the electrode is given in Table 3. Interpass temperatures are maintained to maximum 200 ^{0}C in order to avoid cold cracking on the weld metal and also on HAZ region.

Table 3: Chemical composition and mechanical properties of ISO 14341-A G 42 3m G3Si1 welding electrode

Chemical Composition					Mechanical Properties			
C **min** **max**	**Si** **min** **max**	**Mn** **min** **max**	**P**	**S**	**R_m (MPa)**	**R_s (MPa)**	**A_g %**	**Current Ampere**
0.06 0.14	0.70 1.00	1.30 1.60	0.025	0.025	530	430	24	120-380

During welding procedure plates used for residual stress determination were clamped from four corners as seen in Figure 19. In this figure application of 2-pass welding was also shown.

Figure 19: Application of 2-pass welding

For angular deflection measurement the plates were fixed with 2 clamps from 2 corners of one side (Figure 20). Each weld pass was applied through the whole length of the welding notch. One side of the plate remained not-fixed for deflection measurement.

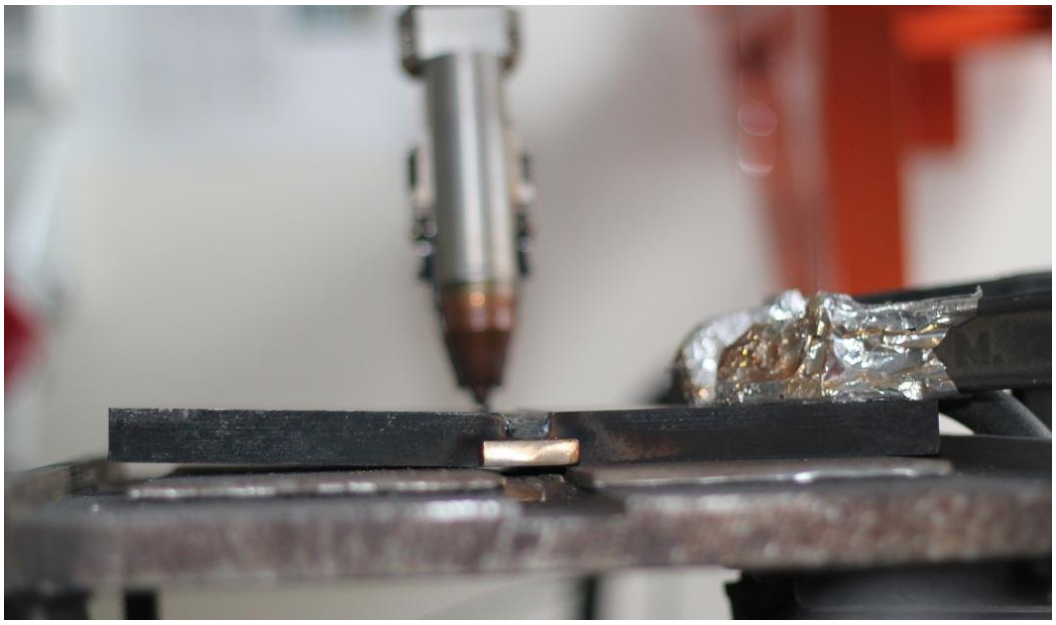

Figure 20: Deflection measurement specimens

3.4 Residual Stress Measurement

During residual stress measurement by MBN using Rollscan / μscan 500-2 instrument with code 4316 probe two methods were used: roll-scan and micro-scan. Residual stress profiles along the sample surfaces were obtained at the rollscan mode. The probe was connected to a motor controlled platform to provide continuous and stable measurement (Figure 21). Probe was stabilized to get fully connected with surface of the test specimen in order to satisfy precise measurement. The plates, set on the motor controlled platform, move under the probe with velocity of 0.2 cm/sec in the horizontal direction. Residual stress measurements were conducted with 125 Hz magnetic field and with a burst rate of 74. Wide band pass filter was set to a range of 1-400 kHz. The received MBN signal was amplified with a gain of 30 dB and the peak magnetization voltage was set to 15V.

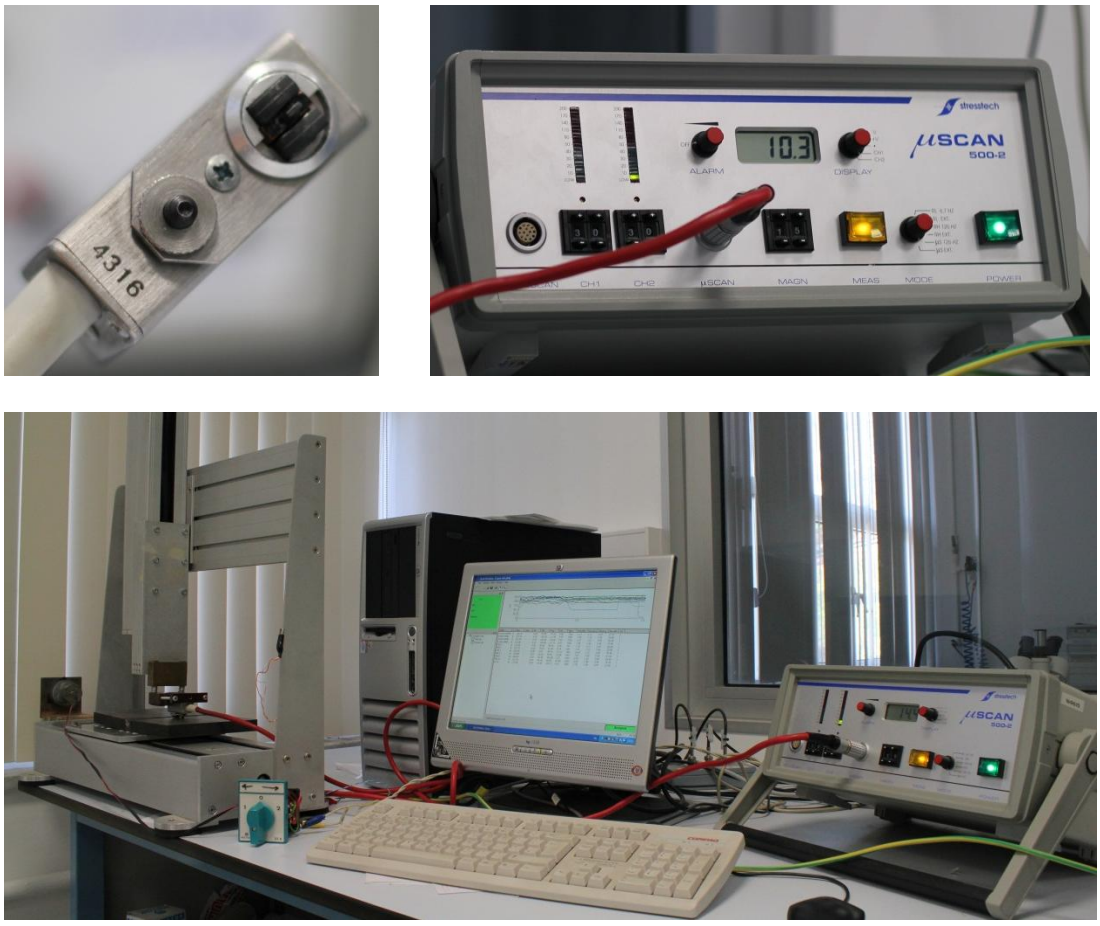

Figure 21: The instrument set-up and 4316 rollscan/microscan probe

Figure 22 shows the schematic view of the measurement lines. To do measurements in a convenient way, the specimen was divided into imaginary sections as well. 2 pass fixed plate was divided into 3 sections with 2 horizontal lines on the other hand 4 and 8 pass plates were divided into 4 sections with 3 horizontal lines.

In these sections each set of line on the horizontal direction is marked with X and each set of line on the vertical direction is marked with Y. Top right corner of the sample set as an origin in x-y coordinate system. At each plate marking was done on the top right corner of the sample to set sample's position relative to the measurement lines. These lines were coded as X1, X2, X3 in the horizontal and Y1, Y2, Y3 in the vertical directions. Since residual stress state is not critical in the metal, to compromise the measurement section horizontally 100mm of distance traveled along X lines for measurement in rollscan mode. Y1 line is set to beginning of measurement distance. Of 100mm along these horizontal lines MBN

measurements were done with Roll-scan method. In addition to these measurements, at the points where horizontal and vertical lines intersect, MBN measurements with micro-scan method were done.

In microscan method frequency and filtering mechanisms are adjustable in contrast to the rollscan method. Using microscan mode HAZ region of specimens were examined and magnetic fingerprints were obtained. Both sides of the plates were examined.

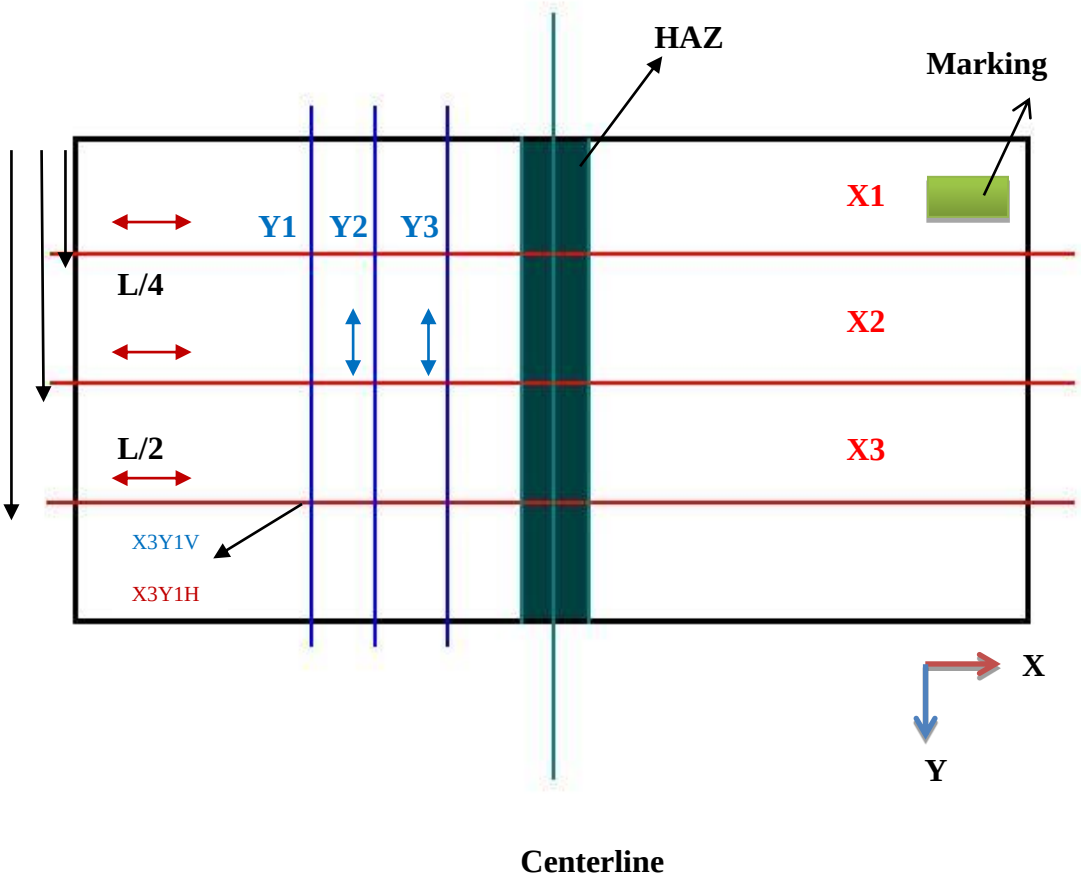

Figure 22: Measurement lines and points

The residual stress measurements were done both for fixed end and non-fixed plates. To avoid probe deformation due to angular deflection done on the deflection specimens, measurements at the deflection specimens were done separately from each side of HAZ of the specimens. To verify the MBN measurements, residual

stresses were measured at 3 points on the welded samples by X-ray diffraction method using Seifert XRD 3003 PTS diffractometer system.

3.5 Calibration Procedure

Calibration procedure was done to transform the MBN data into stress values in MPa unit. Zwick (250 kN) universal testing machine with special attachment that fix 4316 probe on the tensile specimen was used.

The specimen used for calibration was heat treated at 600 ^{0}C for two hours to minimize the compressive residual stress on the surface due to machining. After heat treatment the specimen was connected to turning machine and surface is ground with an emery paper while the specimen turns at low speed. Tensile test results of the specimen after heat treatment were given in Table 4.

Table 4: Tensile test results of the specimen

E (GPa)	**$R_{p0.2}$ (MPa)**	**R_m (MPa)**	**F_m (kN)**	**A_g (%)**	**R_B (MPa)**	**$A_{t(corr)}$ (%)**
205.16	278.97	426.87	33.53	19.10	101.26	42.85

Tensile test results revealed that mechanical properties of the steel decreased dramatically relative to the API standards ($R_{t0.5}$=485MPa, R_m=570 MPa) [1] after the heat treatment.

During MBN measurement obtained unit for measurement was magnetoelastic parameter (MP). Calibration curve for the base metal (Figure 23) was obtained for transforming MP unit into Elastic Tensile Stress in MPa units.

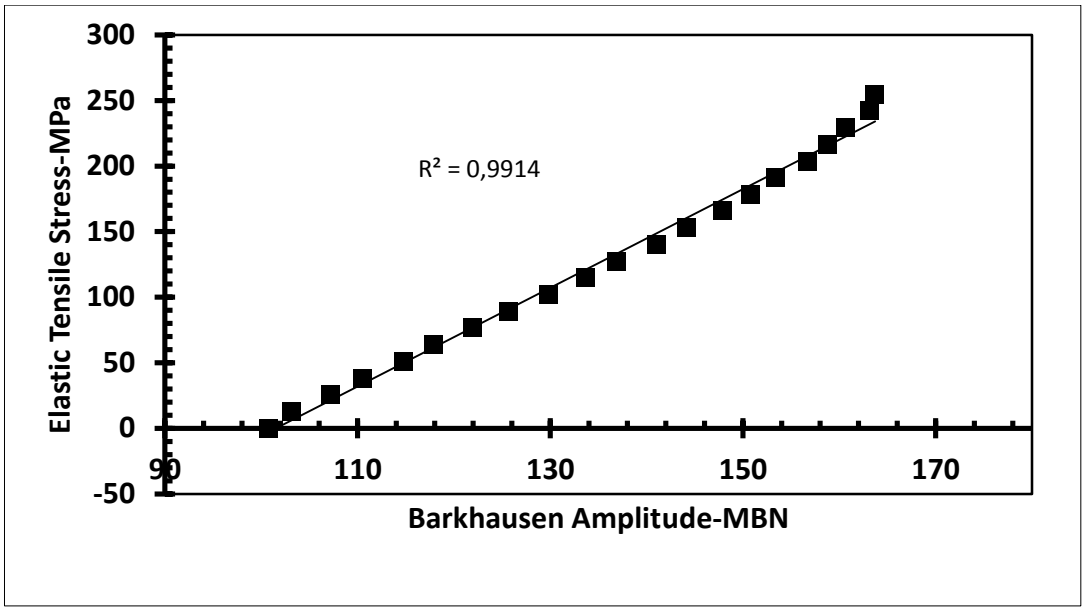

Figure 23: Calibration curve for the base material

3.6 Angular Deflection Measurement

Amount of angular deflection $\Delta\theta$ at the free-end specimens is given in Equation 5;

$$2\Delta\theta = \sin(\alpha / b) \qquad 5$$

In the Equation 5, α is the displacement of the unclamped side of the material along Y-axis and b is the half length of the specimen along X-axis.

Steel plate was assumed to give the same deflection at both sides. One side of the plate fixed to the ground so the deflection angle found is $2\Delta\theta$.

3.7 X-Ray Diffraction Measurement

XRD measurements were done to control the coherency of calibrated RS data obtained by MBN method. XRD measurements were conducted by SEIFERT XRD 3003 PTS diffractometer system. Cog: Mean method was applied to study the state of residual stress. The incident X-Ray Cr-K_α beam directed to acquire data form the (211) α-Fe diffraction line profiles. Effective penetration depth of Cr radiation into steel for the (211) peak is nearly 5 microns [48].

CHAPTER 4

RESULTS

4.1 Microstructure and Hardness Results

Macrostructure examination of three API 5L X-70 steel plates with 2,4 and 8 weld pass were done to clearly see the effect of number of passes on macro level. Microstructure investigation of steel plates were done from the base metal of all fixed- end specimens from the surface perpendicular to the back surface of the specimen. Microstructural examinations were conducted with Olympus PME 3 After the metallographic examination it was determined that HAZ region for each pass changes within 2.1mm and 2.5mm.

Hardness examination was conducted with 1 mm separation along 20 mm in both right and left directions relative to weld centerline. It was done from cross-section of each specimen's base material. It was positioned under the weld centerline at the edge where back surface of the specimen and cross-section intersects. For hardness examination Shimadzu HMV-2 Micro Hardness Tester was used. 2 kg (19.6N) of load was applied to the specimens for 10 seconds.

Microstructure investigations were done according to ASTM E112 standard [49]. Number of grains per mm^2(N_A), mean grain cross sectional area(A) and ASTM grain size number(G) are the parameters which reveal that no grain coarsening observed at the back of the surface.

Microstructure investigation perpendicular to surface in which residual stress obtained, was also conducted. Base metal, HAZ and weld metal sections were also shown. Macrographs of the specimens were obtained by using a computer scanner with an image quality of 4800 dpi.

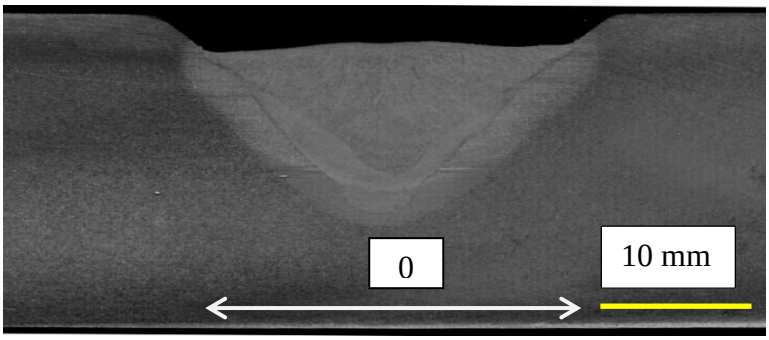

Figure 24: Macrograph of the 2 pass welded API 5L X-70 steel

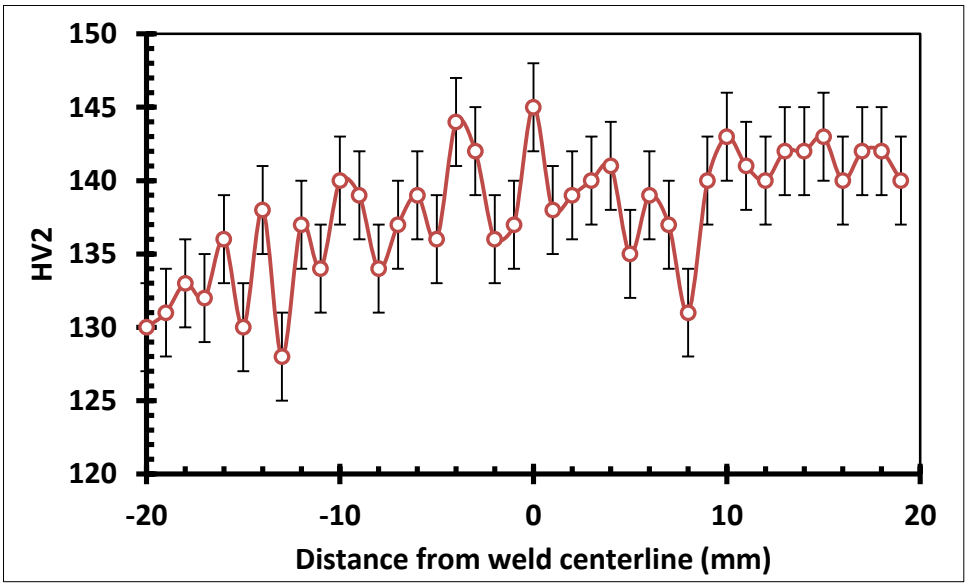

Figure 25: Hardness profiles of the 2 pass welded plate (back surface)

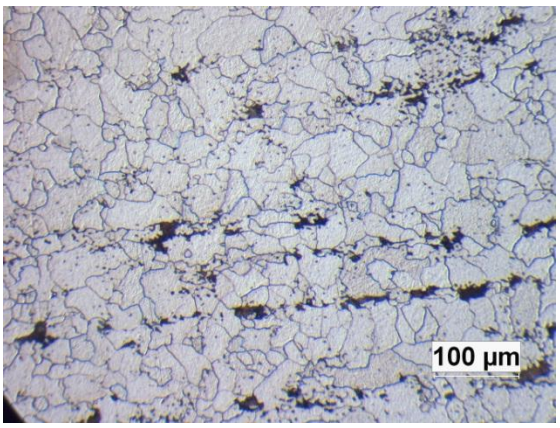

N_A= number of grains per mm^2 at 1X

A = mean grain cross sectional area

G = ASTM grain size number

N_A= 89

A = 0.0112

G = 3.5

Figure 26: Representative micrograph of the 2 pass welded plate

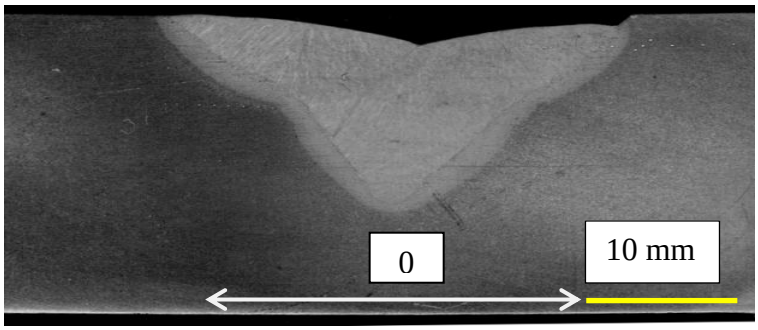

Figure 27: Macrograph of the 4 pass welded API 5L X-70 steel

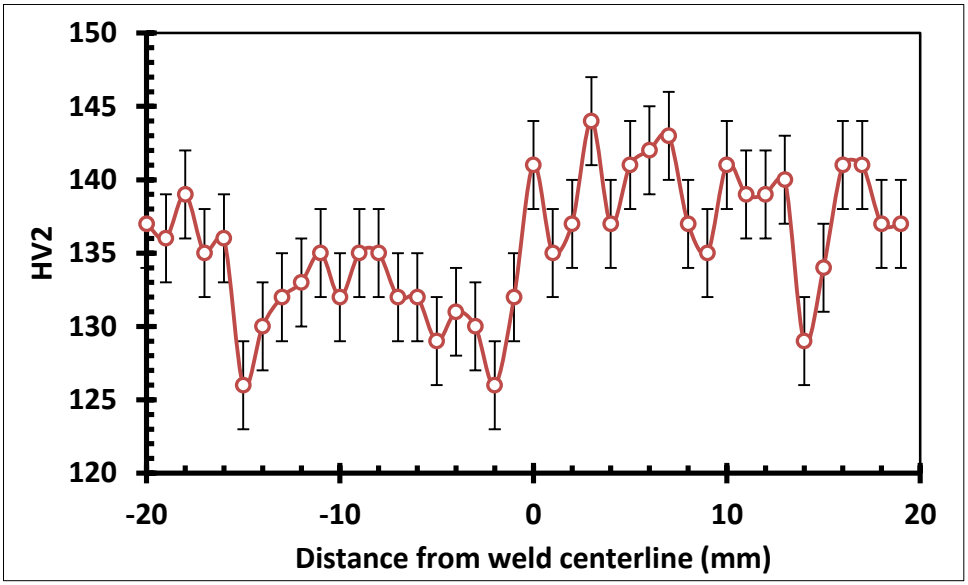

Figure 28: Hardness profiles of the 4 pass welded plate (back surface)

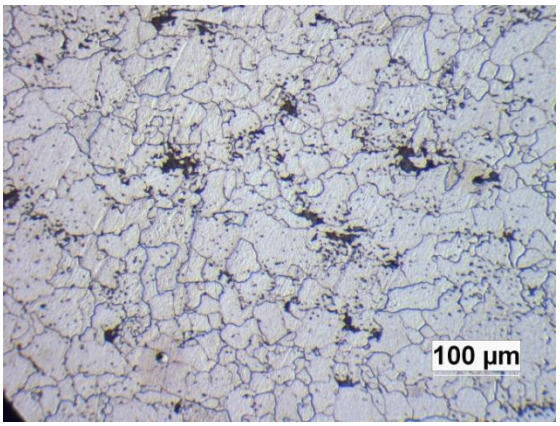

N_A= number of grains per mm^2

at 1X

A = mean grain cross sectional area

G = ASTM grain size number

N_A= 88

A = 0.0114

G = 3.5

Figure 29: Representative micrograph of the 4 pass welded plate

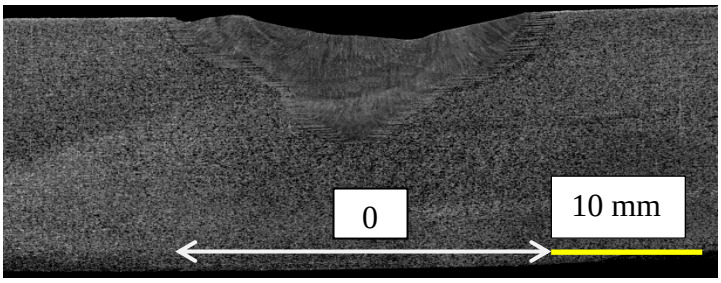

Figure 30: Macrograph of the 8 pass welded API 5L X-70 steel

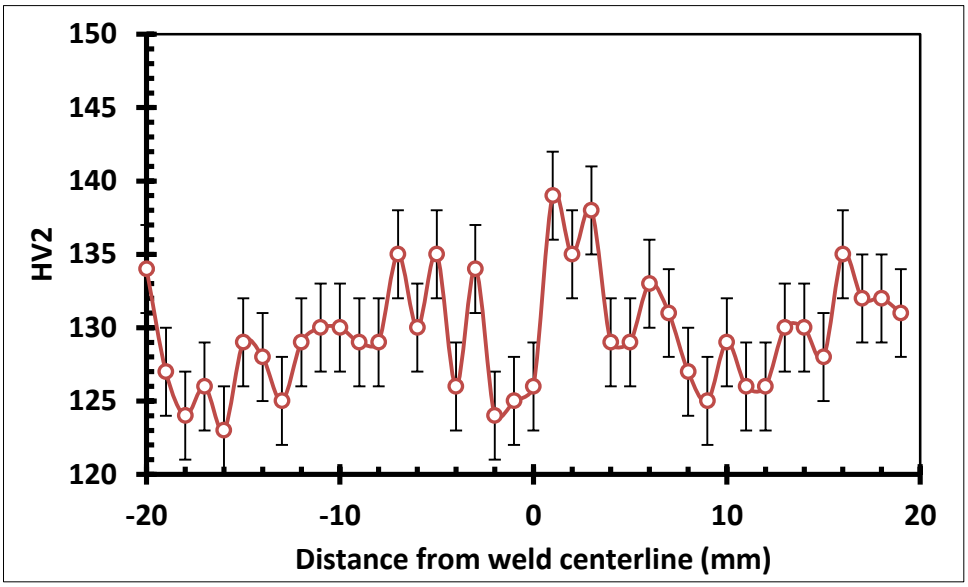

Figure 31: Hardness profiles of the 8 pass welded plate (back surface)

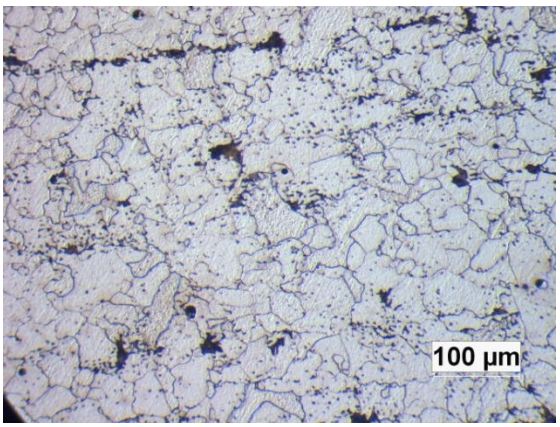

N_A= number of grains per mm^2 at 1X

A = mean grain cross sectional area

G = ASTM grain size number

N_A= 91

A = 0.0110

G = 3.5

Figure 32: Representative micrograph of the 8 pass welded plate

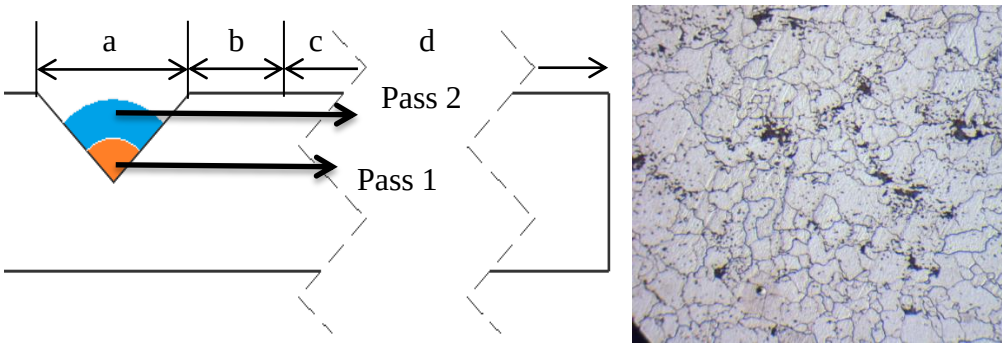

Figure 33: Schematic view of the weld passes and microstructure parent metal microstructure of 2 pass API 5L X-70 steel

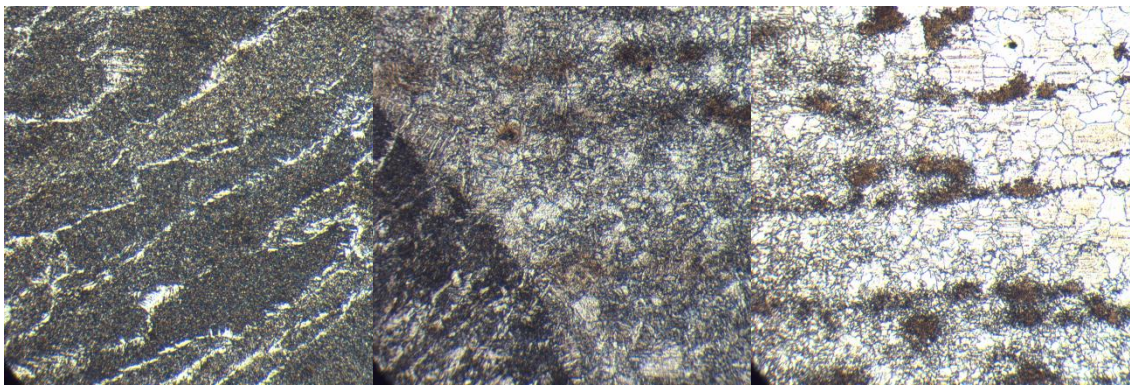

Weld (a) Weld to HAZ (b-c) HAZ to Parent (c-d)

Figure 34: Microstructure after 1st weld pass (for 2-pass welded plate)

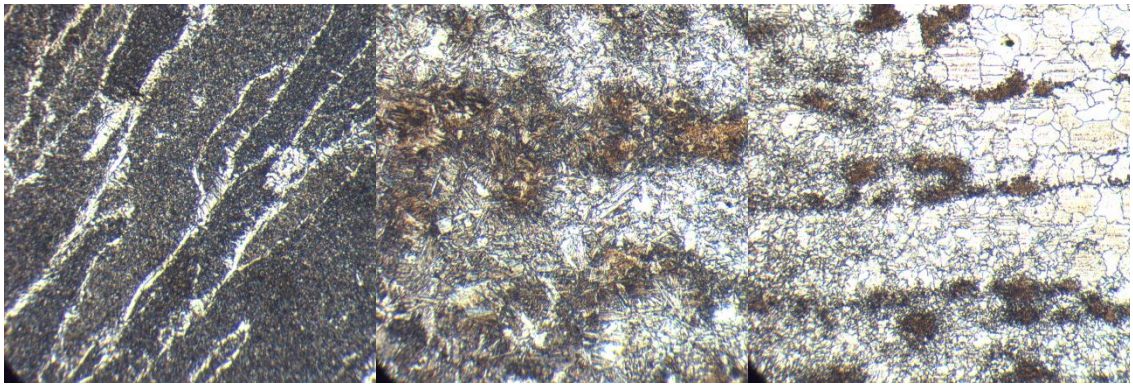

Weld (a) Weld to HAZ (b-c) HAZ to Parent (c-d)

Figure 35: Microstructure after 2nd weld pass (for 2-pass welded plate)

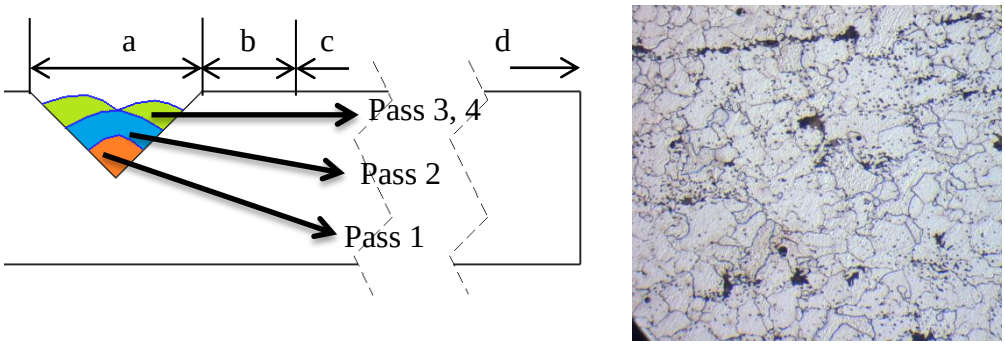

Figure 36: Schematic of weld passes and parent metal microstructure of 4 pass API 5L X-70 steel

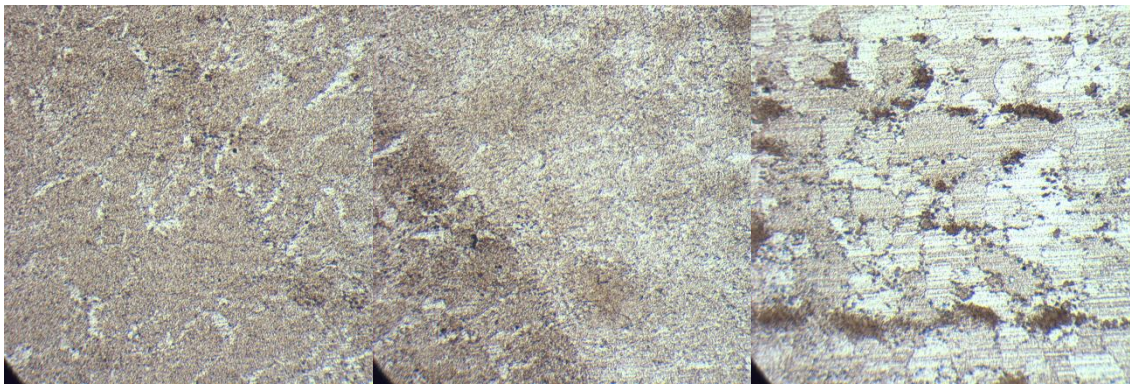

Weld (a) Weld to HAZ (b-c) HAZ to Parent (c-d)

Figure 37: Microstructure of 1st weld pass (for 4-pass welded plate)

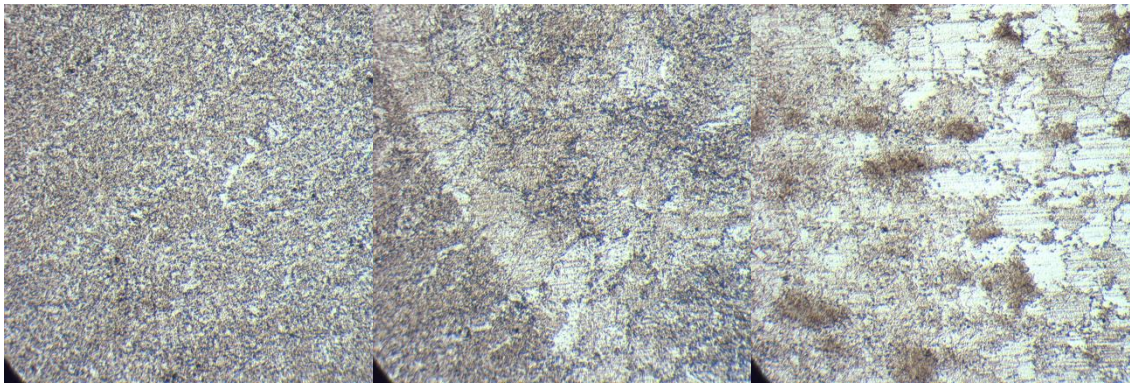

Weld (a) Weld to HAZ (b-c) HAZ to Parent (c-d)

Figure 38: Microstructure of 2nd weld pass (for 4-pass welded plate)

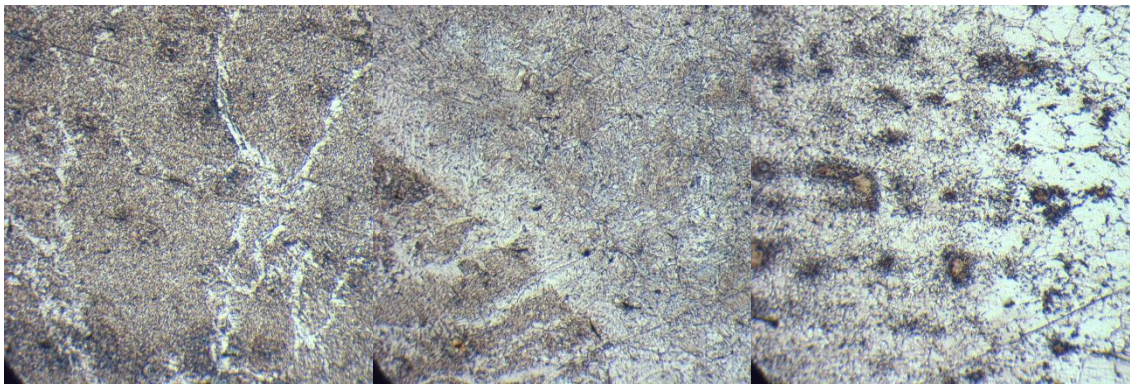

Weld (a) Weld to HAZ (b-c) HAZ to Parent (c-d)

Figure 39: Microstructure of 3rd and 4th weld pass (for 4-pass welded plate)

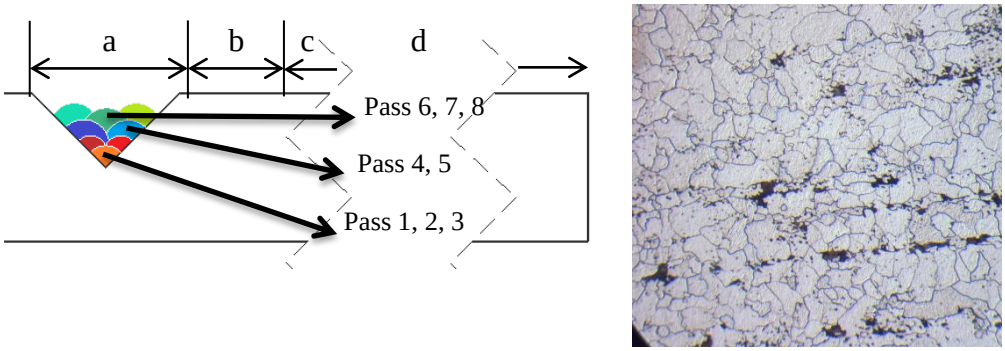

Figure 40: Schematic of weld passes and parent metal microstructure of 8 pass API 5L X-70 steel

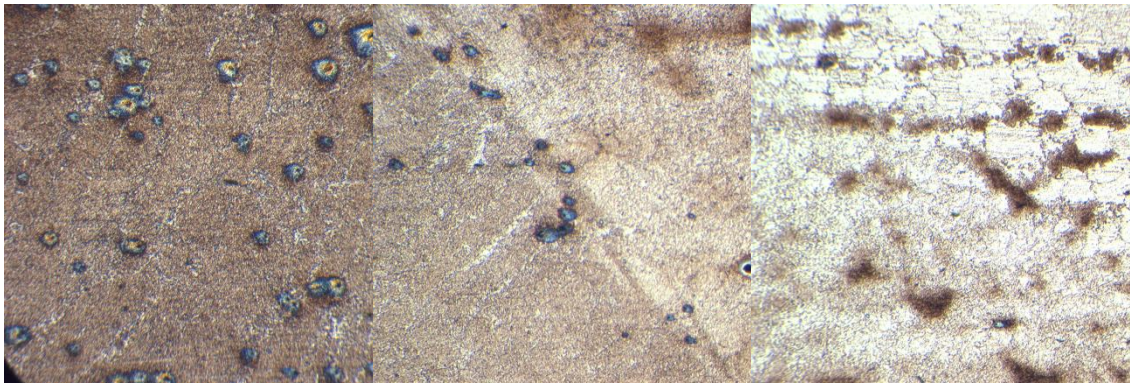

Weld (a) Weld to HAZ (b-c) HAZ to Parent (c-d)

Figure 41: Microstructure of 1st, 2nd and 3rd weld pass (for 8-pass welded plate)

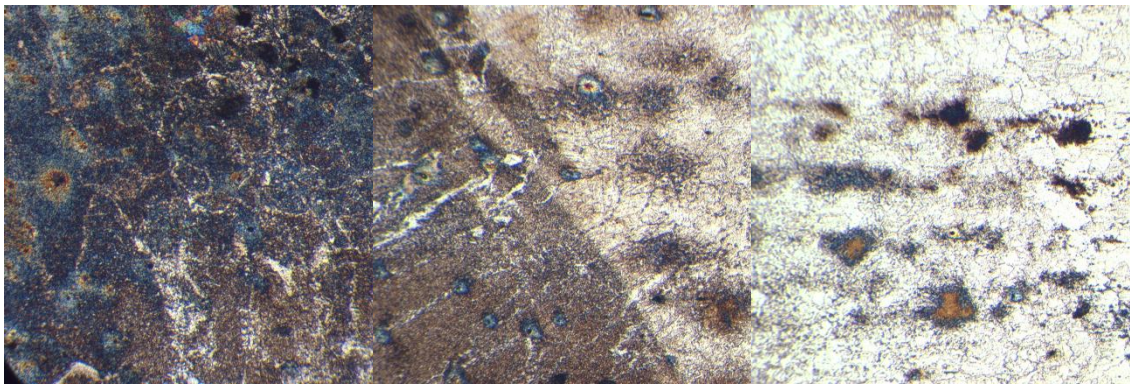

Weld (a) Weld to HAZ (b-c) HAZ to Parent (c-d)

Figure 42: Microstructure of 4th and 5th weld pass (for 8-pass welded plate)

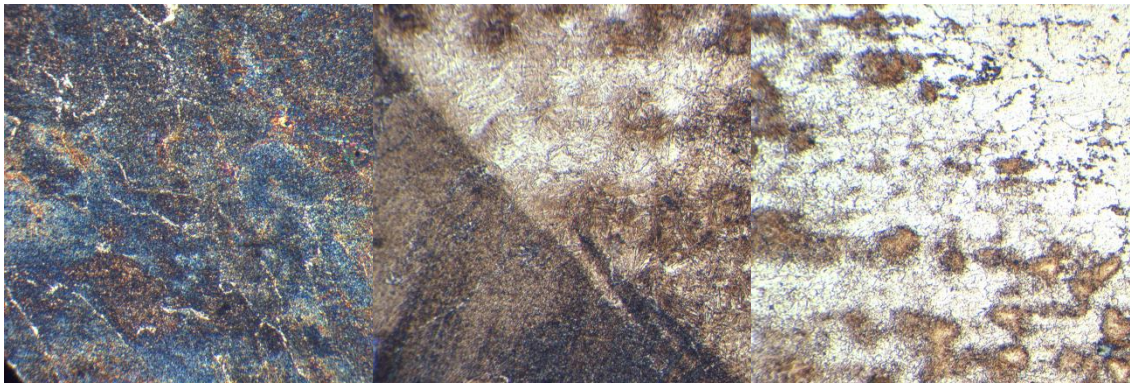

Weld (a) Weld to HAZ (b-c) HAZ to Parent (c-d)

Figure 43: Fig Microstructure of 6th, 7th and 8th weld pass (for 8-pass welded plate)

4.2 MBN Results for Base Metal Calibration

Figure 44, Figure 45 and Figure 46 show continuous residual stress measurement results of 2 pass, 4 pass, 8 pass welded fixed-end API 5L X-70 steel from front surface. Figure 47 shows continuous residual stress results of final passes for fixed-end API 5L X-70 steel from front surface.

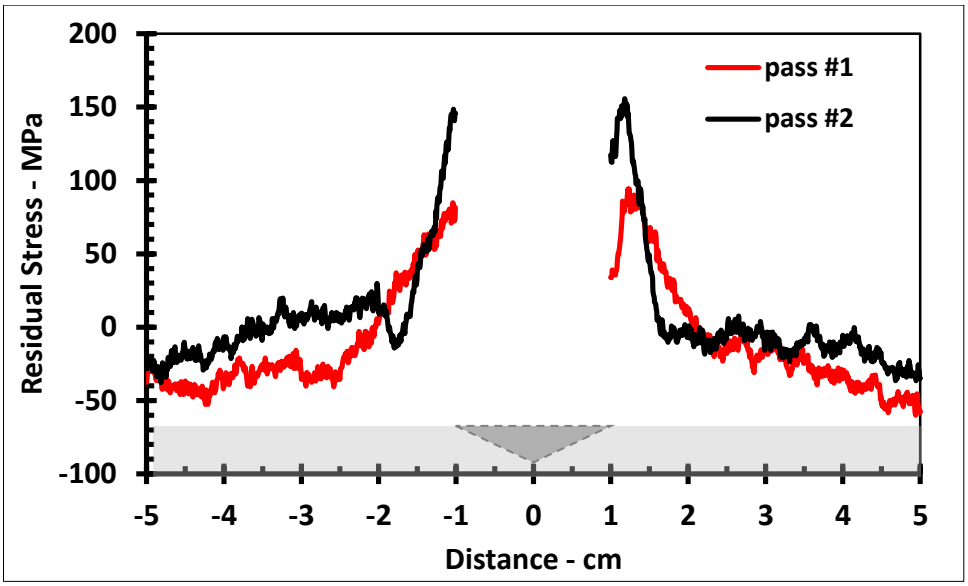

Figure 44: Residual stress profiles at the front surface (2-pass welded; fixed-end)

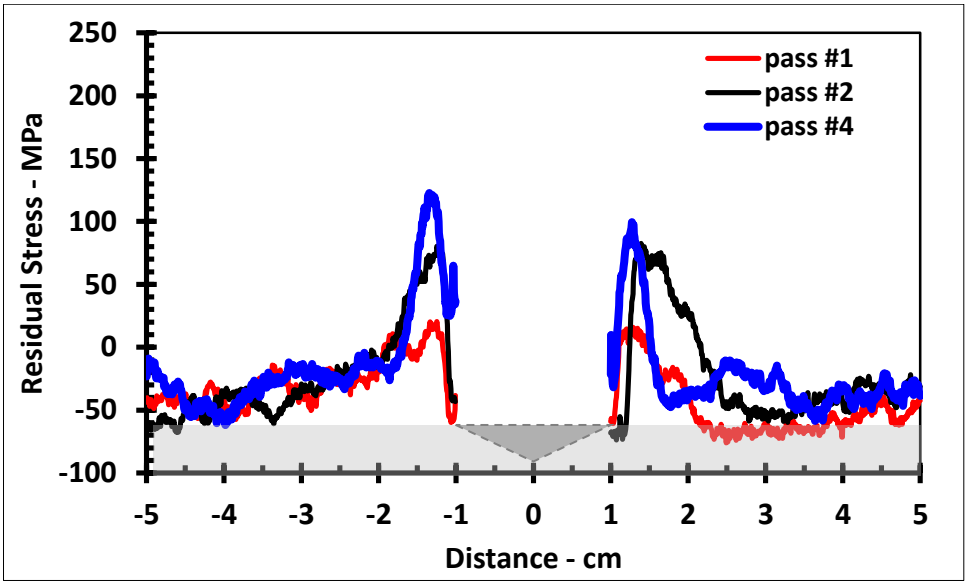

Figure 45: Residual stress profiles at the front surface (4-pass welded; fixed-end)

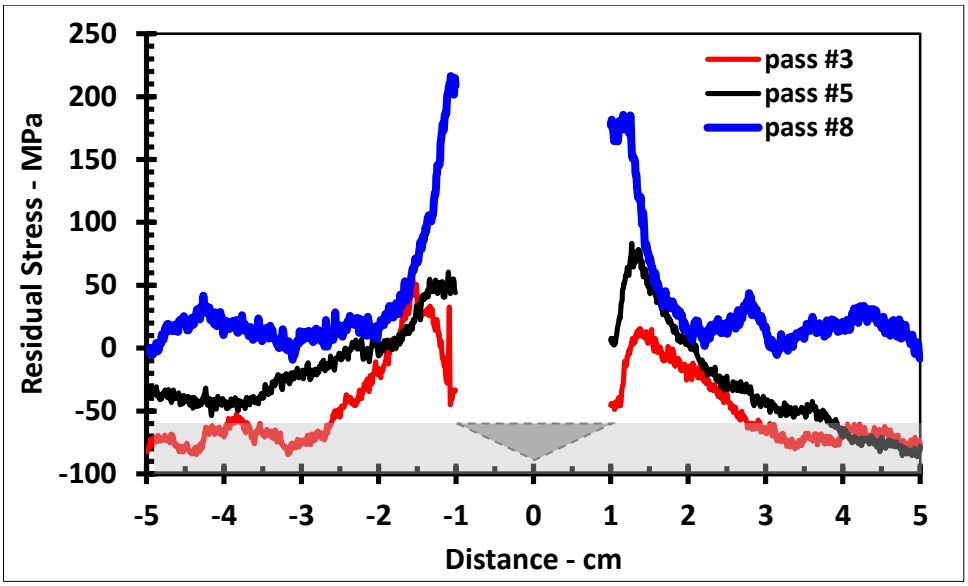

Figure 46: Residual stress profiles at the front surface (8-pass welded; fixed-end)

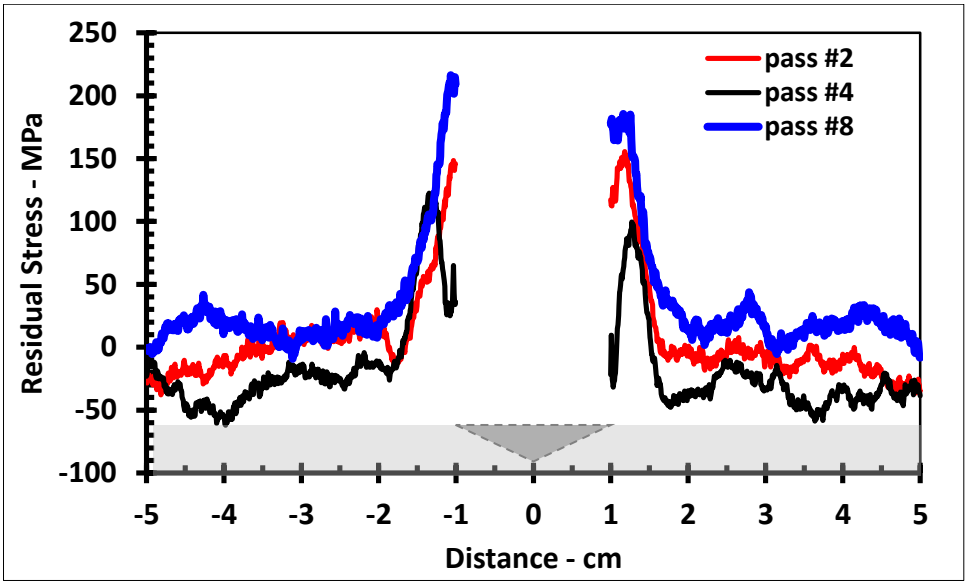

Figure 47: Residual stress profiles at the front surface (final weld passes; fixed-end)

Figure 48, Figure 49 and Figure 50 show continuous residual stress measurement results of 2 pass, 4 pass, 8 pass welded API 5L X-70 steel from back surface. Figure 51 shows continuous residual stress measurement results final weld passes for API 5L X-70 steel from back surface.

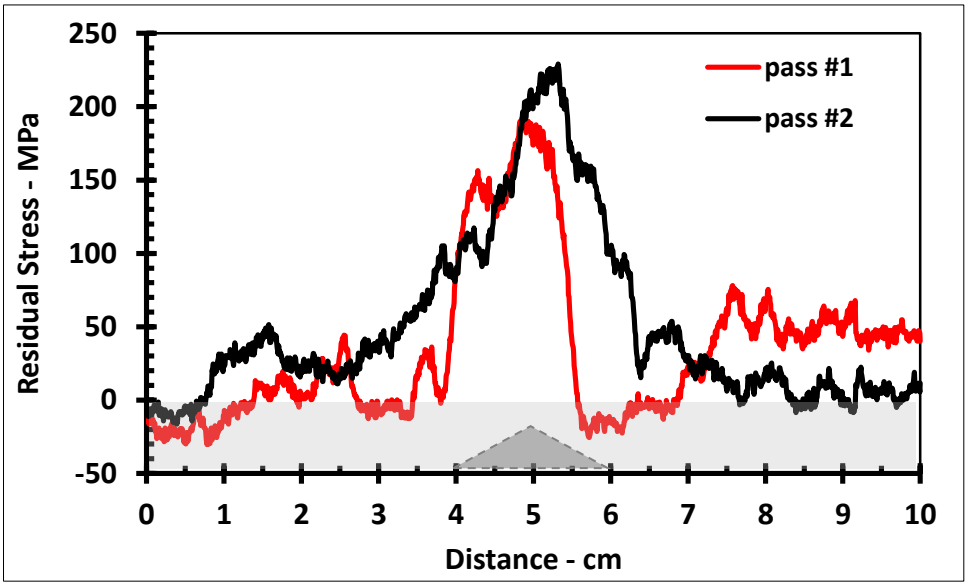

Figure 48: Residual stress profiles at the back surface (2-pass welded; fixed-end)

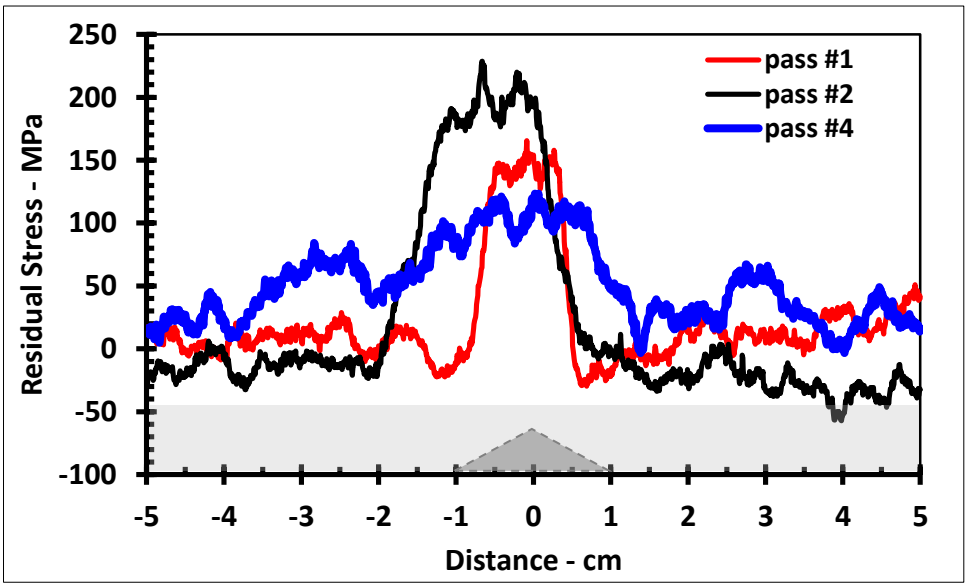

Figure 49: Residual stress profiles at the back surface (4-pass welded; fixed-end)

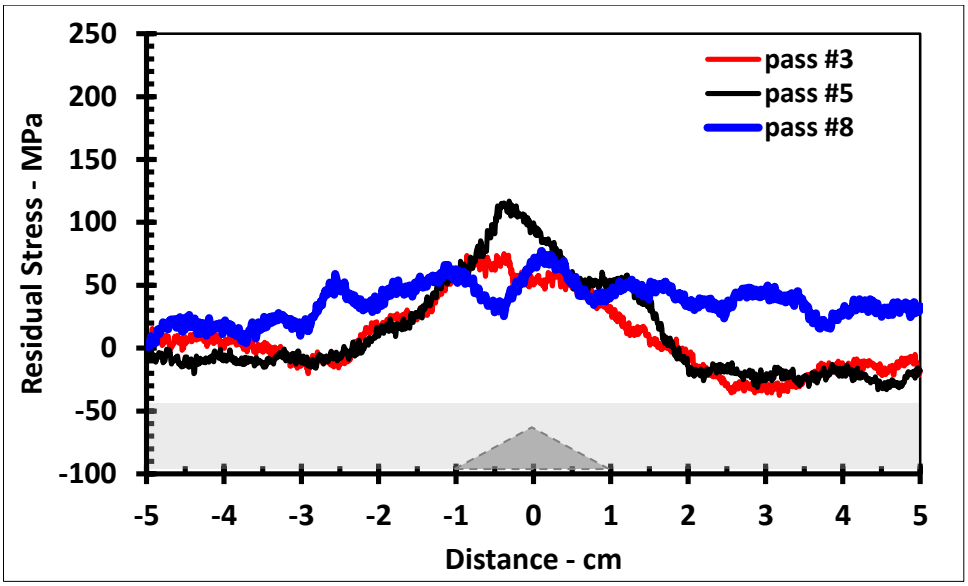

Figure 50: Residual stress profiles at the back surface (8-pass welded; fixed-end)

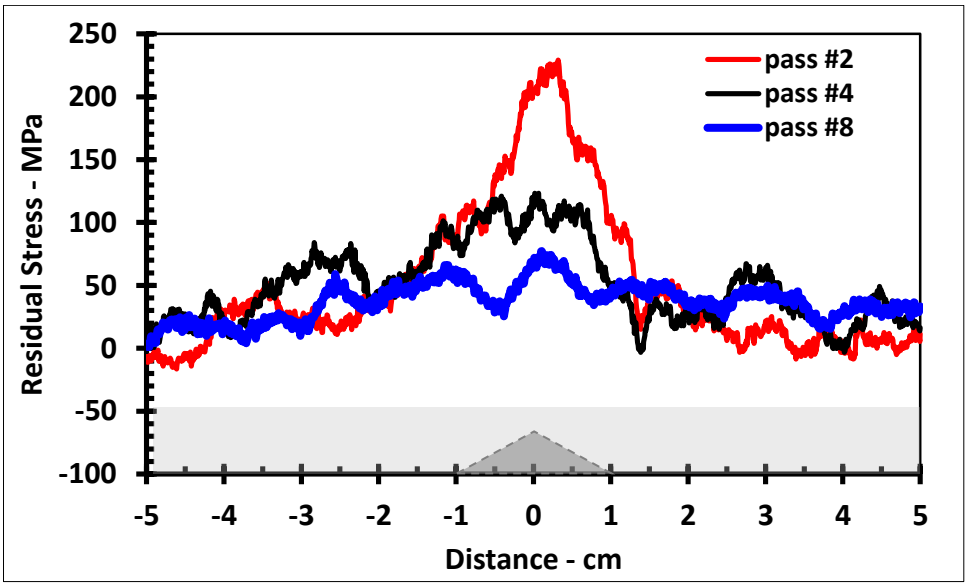

Figure 51: Residual stress profiles at the back surface (final weld passes; fixed-end)

In Figure 52, Figure 53 and Figure 54 MBN profiles of fixed-end specimens are given. MBN profiles are taken from weld centerline of the weld pass of each specimen.

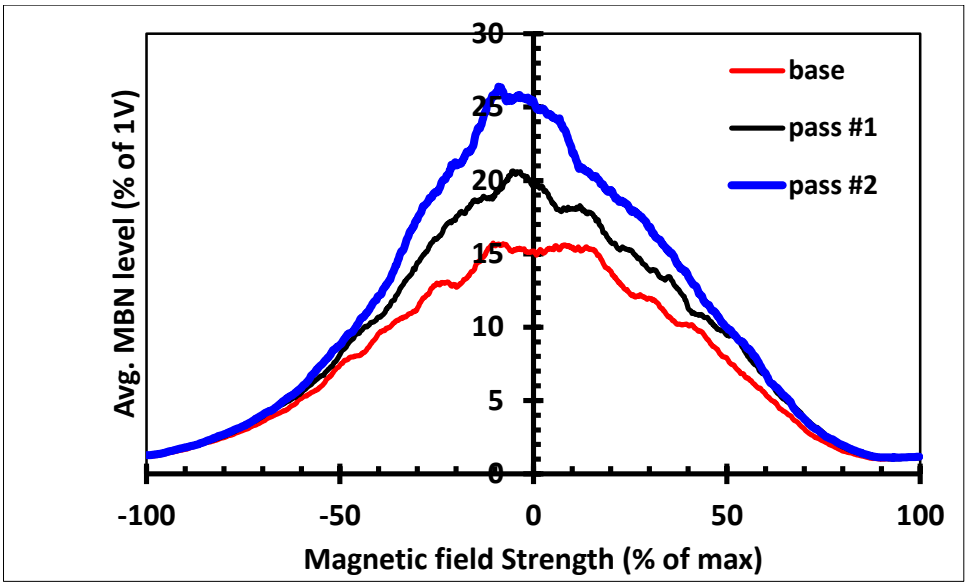

Figure 52: MBN profiles (fingerprints) at the back surface (2-pass welded; fixed-end)

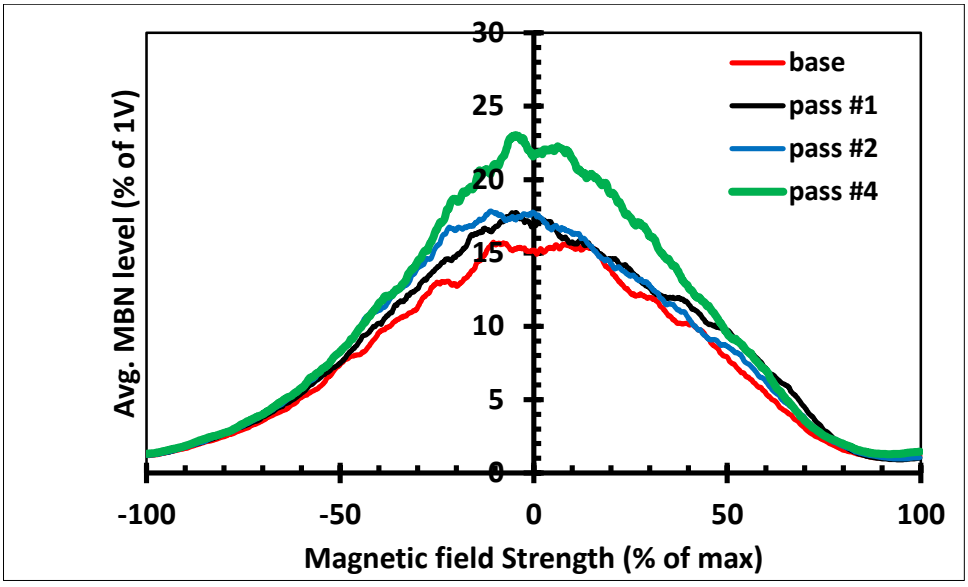

Figure 53: MBN profiles (fingerprints) at the back surface (4-pass welded; fixed-end)

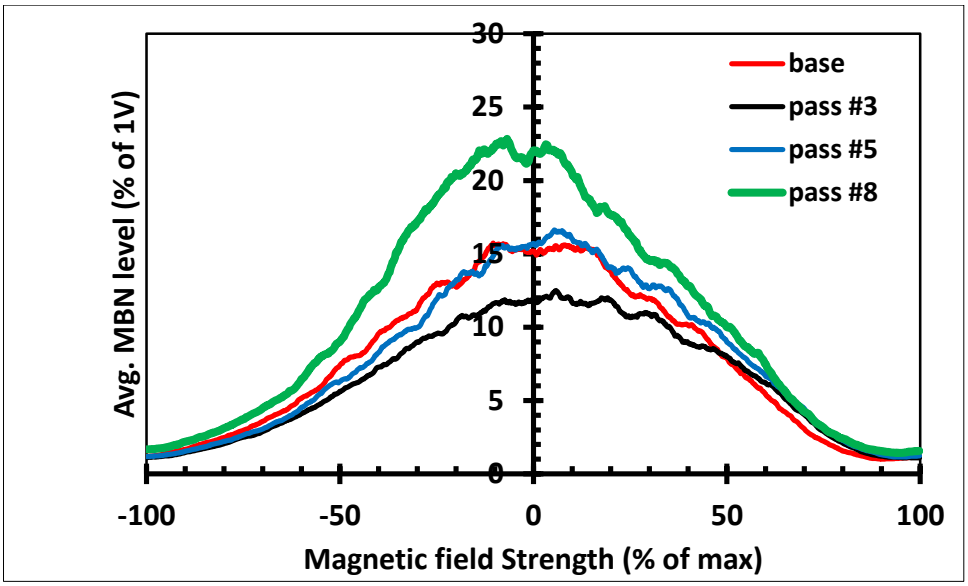

Figure 54: MBN profiles (fingerprints) at the back surface (8-pass welded; fixed-end)

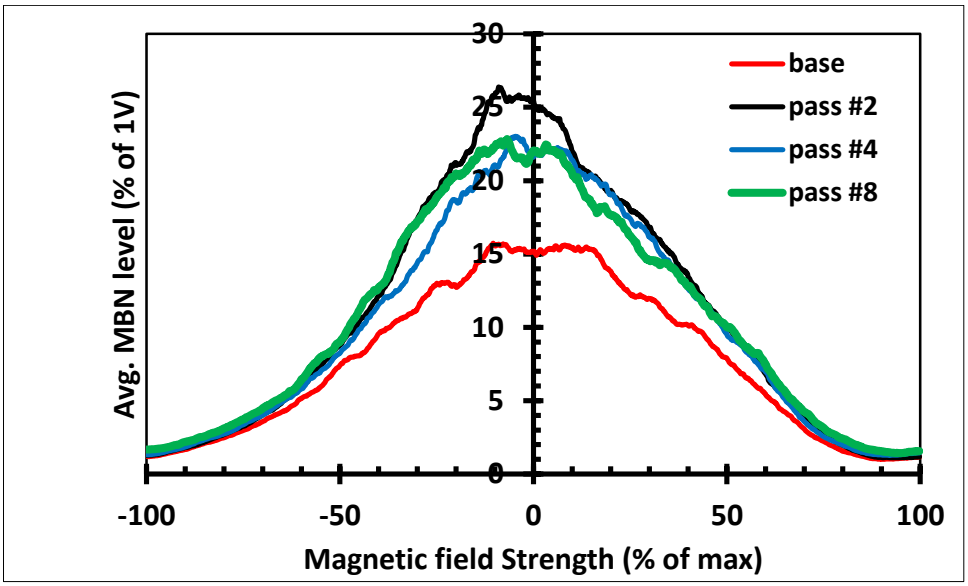

Figure 55: MBN profiles (fingerprints) at the back surface (final weld passes; fixed-end)

4.3 Deflection Results

In table 5, angular deflection values of the free-ended plates are given.

Table 5: Angular deflection data of free-ended plates

Number of pass	Deflection h (mm)	Degree
1	3,5	1,4
2	6,1	2,5
1	2,1	0,9
2	4,1	1,7
4	5,9	2,4
3	4,4	1,8
5	4,8	2,0
8	4,9	2,0

Barkhausen amplitude-MBN, angular deflection and heat input shows correlation between each other. In Figure 56, relationship of MBN with number of passes, in Figure 57 relationship of angular deflection with number of passes and Figure 58 in relationship of heat input with number of passes is given.

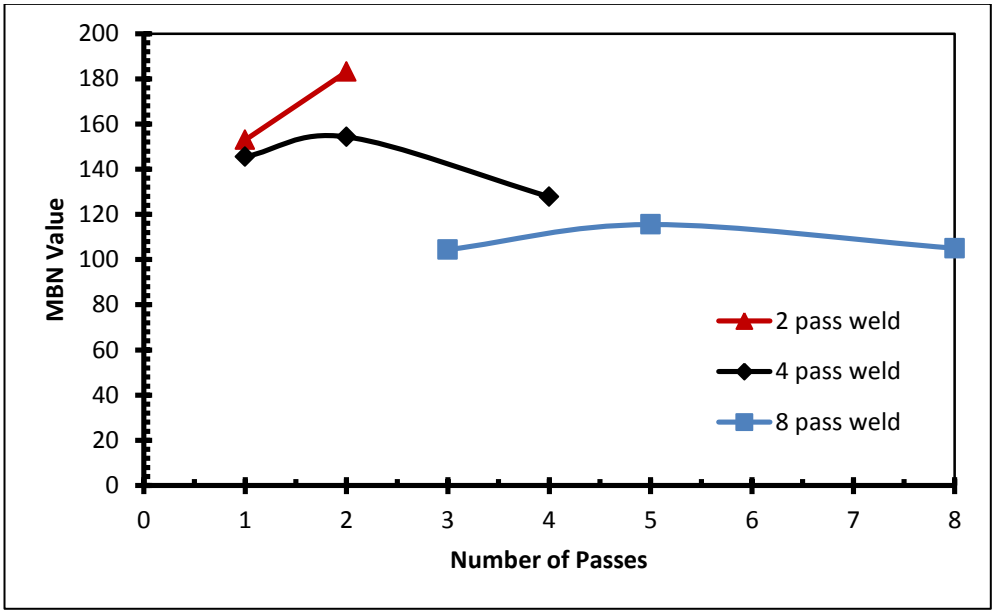

Figure 56: Barkhausen amplitude-MBN vs. number of passes

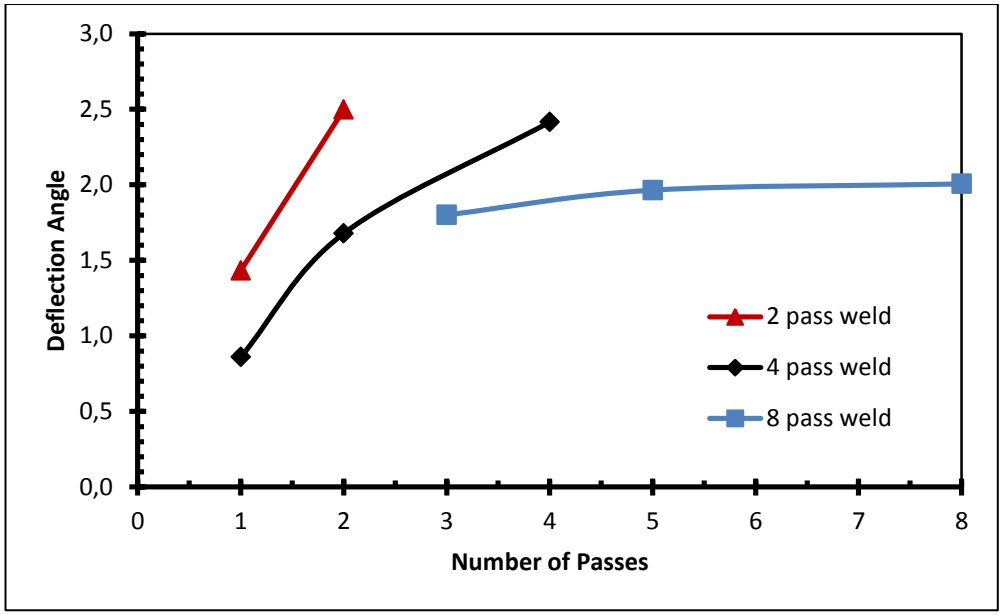

Figure 57: Angular deflection vs. number of passes

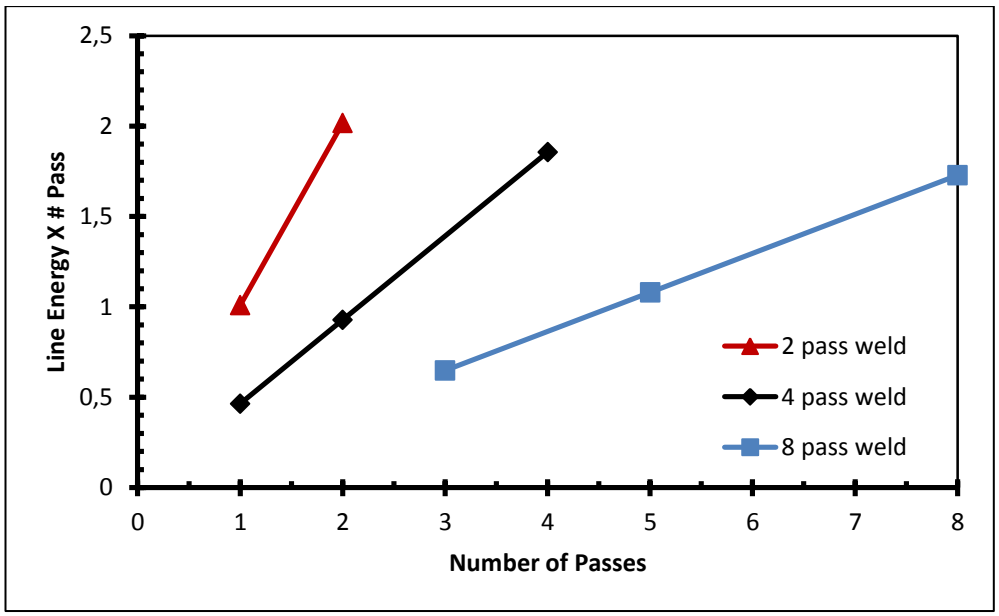

Figure 58: Heat input vs. number of passes

In Figure 59 and Figure 60 residual stress results and MBN profiles of final weld passes of 2, 4 and 8 pass welded free-end from back surface are given. Deflection

results are taken after the final pass of each welding sequence ended in order not to change the strain status of the fixed end specimens.

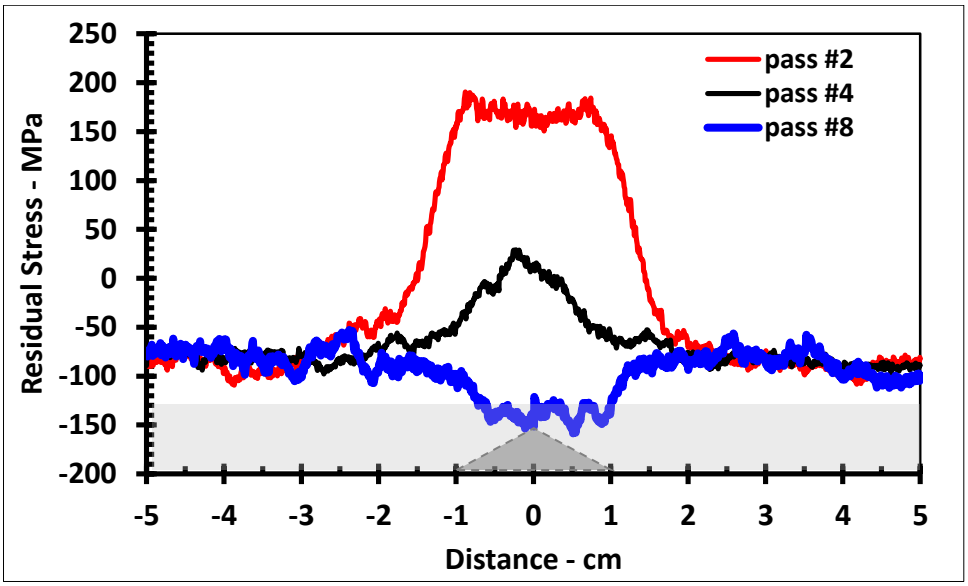

Figure 59: Line profile of the back surface residual stresses from after the final weld-passes (free-end)

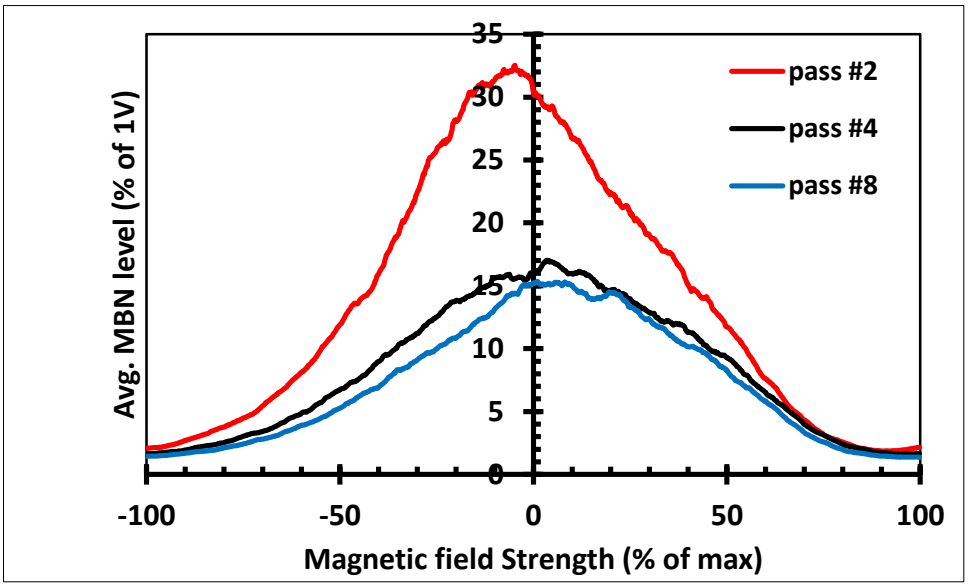

Figure 60: MBN profiles (fingerprints) at the back surface (final weld passes; free-end)

4.4 Verification of MBN results by X-Ray Diffraction Method

MBN methods requires verification in order to determine whether calibration is correct or not X- Ray measurement is done on 4 pass welded specimen from the 4th weld pass. In Figure 61 comparison of the residual stresses measured by X-Ray diffraction measurement and Barkhausen noise method is given. CoG: Mean method was applied to study the state of residual stress. Cr-K_α radiation X-ray beam directed to acquire data form the (211) α-Fe diffraction line profiles.

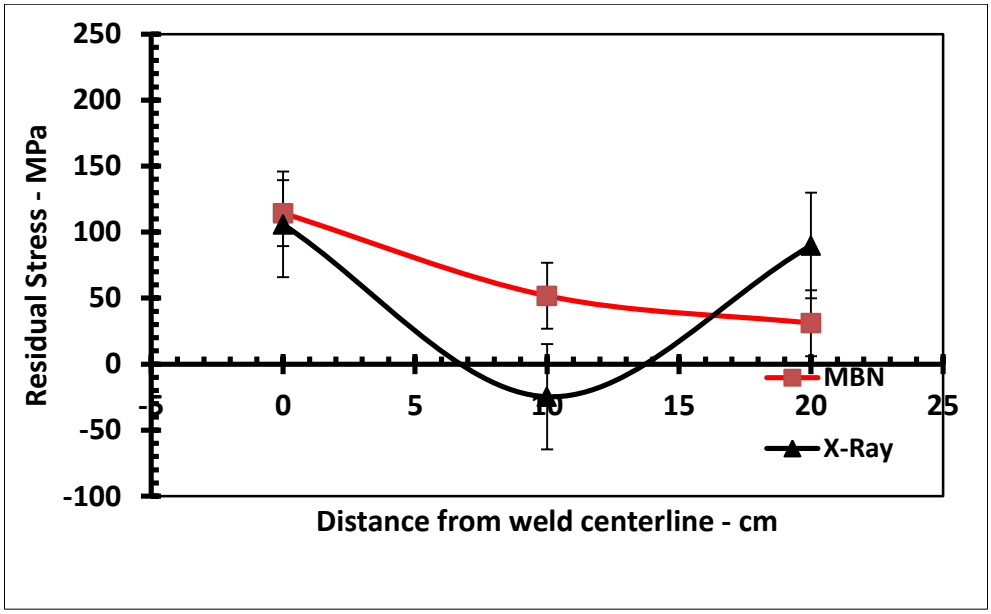

Figure 61: Comparison of residual stress values for X-Ray diffraction and Barkhausen Noise

CHAPTER 5

DISCUSSION

5.1 Microstructure and Hardness

All specimens followed the same heat treatment route and welding was carried out on V-notch without full penetration, microstructural differences on the back surface were not expected.

As expected, the back surfaces of all 2, 4 and 8 pass welded samples have the similar microstructure (the number of grains per mm2 at 1x magnification is between 88 and 91; and the mean grain cross-sectional area is between 0,0110 and 0,0114), the same ASTM grain size number (G value is 3,5), and their hardness values are within the range of 135 and 140 HV as seen in Figure 25, Figure 28 and Figure 31. Also HAZ characteristics of the specimens are similar (2.1 - 2.5 mm) as seen in Figure 33 to Figure 43.

Hardness values are in the range of same order. These values are relatively low compared to as received state of the material. Low hardness values are in tandem with the mechanical properties obtained from the tensile test ($R_{p0.2}$=279MPa, R_m=427 MPa), because tensile strength and other mechanical properties are relatively low compared to the standards for API 5L X-70 steel ($R_{t0.5}$=485MPa, R_m=570 MPa) [1]. The low values of hardness and strength stem from the annealing treatment (960 C^0 / 1.5 hrs.) that was applied to eliminate the variational effect of microstructure on MBN emission.

MBN emission contains combined information of the residual stress state and microstructure [26]. Each three sample basically showed the same characteristic of

Vickers hardness statue. Since microstructure and composition of the plates are constant for the back surfaces, residual stress state is the dominant factor that affects the MBN response.

5.2 MBN results

MBN results were converted to the residual stress values based on parent metal calibration. Although Yelbay applied both parent metal based and HAZ based calibration [25] to achieve most suitable calibration procedure, HAZ based calibration was not applied in this study because it was impractical to apply different calibration procedure for different specimens with varying number of weld passes for the validity of the experiment. MBN measurements were conducted from both front and back side of the fixed-end specimens. The measurements were conducted from only back side of the free-end specimens. Because distorted specimens did not allow probe to connect to the surface in a proper way. Residual stress profiles at each side of the plate for both fixed-end and free-end specimens were obtained for a length of 5cm along both directions relative to the weld line.

As a result of nature of welding procedure, thermal gradient is the main source of residual stress formation [7]. Within HAZ where the temperature exceeds the critical values for phase transformations, transformation-induced residual stresses occur. When the effect of phase transformations is dominant compressive residual stresses form in the transformed areas [33]. MBN measurements revealed that maximum tensile residual stress exist at the border between the weld metal and HAZ; and as going to the parent metal through HAZ the magnitude of tensile residual stress decreases, and then, it becomes compressive.

Residual stress profiles from the front surfaces and back surfaces gave a different tendency for variation of residual stress profile as a function of weld passes. For the final weld passes of the front surface as number of weld pass increases amount of tensile residual stress (RS) also increases (Figure 47). As shown in Figure 44, Figure 45 and Figure 46, the highest tensile residual stresses exist near the weld centerline. This result is in agreement with the previous studies [7] [13] which state that compressive residual stresses exist in the HAZ and tensile residual stresses in the

weld metal; tensile residual stresses at the weld centerline are balanced by the compressive stresses at the HAZ; the maximum tensile residual stress was found at the interface between HAZ and the weld metal.

Residual stress profiles from the back surfaces gave a different tendency for variation of residual stress profile as a function of weld passes. Because the microstructure is not a variable for the back surfaces, the residual stress state is the main factor that affects the MBN response obtained from back-sides of the specimens. Residual stress distributions of the 2 pass, 4 pass, 8 pass welded plates are given in Figure 48, Figure 49 and Figure 50 for the back surfaces. After the final weld-pass, the magnitude of the tensile residual stress is lower than those of the prior passes for the back surface as seen in Figure 51. This could be related with the stress-relieving effect of the heat of the successive runs. It is an expected result because most of the heat supply due to welding is moved by conduction through the plate. The plates used in the experiments have a surface area of less than $1m^2$. The real steel pipeline system has enormous surface area compared to the plates used in the experiments. Welding heat supply is imprisoned due to low conduction ability and convection is not an appropriate way to transfer that amount of heat from plate to the environment. Thus, relaxation occurs at the tensile residual stress state of the plate.

For the back surface of free-end specimens, as total number of weld pass increases the magnitude of the tensile residual stress gets lower than those of the prior passes, and finally, residual stress state became compressive for the 8^{th} pass as seen in Figure 59. This could be related with both tempering effect due to heat input of the successive runs and amount of angular deflection which reduces the magnitude of the residual stresses.

MBN profiles peak position gives information on the residual stress state of the material [47]. The MBN profiles (fingerprints) of the fixed-end samples show that as a function of subsequent passes the MBN peak height increases although the required magnetic field strength remains nearly the same (Figure 52, Figure 53 and Figure 54). This increase in peak height reveals that in generally the effective surface area of pinning sites decreases. Moreover, domain walls move more easily because average distance between pinning sites increases. MBN fingerprints of the final weld pass of the shows different tendency for both fixed-end and free-end plates as shown in

Figure 55 and Figure 60; as the total number of weld passes increases MBN peaks drop to the lower emission values.

5.3 Deflection Results

Heat input, welding travel speed [8], and the number of weld passes [9] are important parameters for determining the final distortion of the welded component. Barkhausen amplitude, angular deflection and heat input are given as a function of weld pass number in Figure 56, Figure 57 and Figure 58. As number of passes increases, amount of Barkhausen amplitude and angular deflection reduces. Angular deflection values obtained at this experiment is between 1.4^0 and 2.5^0as seen in

Table 5. These values were relatively low compared to butt welding procedures. Since it was known that the expected angular deflection values are relatively low, for more precise measurements, plates were clamped from one side during welding and angular distortion measurements.

Residual stress profiles of distorted specimens at the back surfaces showed the same characteristics as the fixed-end plates. As number of passes increases, tensile residual stress decreases. However, a different tendency was observed for the 8 pass plate. This plate showed compressive residual stress while 2 pass and 4 pass plates had tensile residual stress in a decreasing manner.

5.4 Verification of Results

X-Ray diffraction measurements were conducted in order to verify the residual stress measurements with MBN method. X-ray diffraction measurements were done on the back surface of the 4-pass welded specimen. In Figure 61 comparison of the residual stresses measured by X-Ray diffraction and MBN method is given. Results are generally in agreement with each other within an acceptable difference range. It should be considered that the results were obtained from different volume of materials because each method has different surface penetration. Depth of MBN signal is about 0.02 to 0.30mm [18] whereas the penetration depth of Cr radiation

into steel for the (211) peak is nearly 5 microns [48]. Moreover for the X-ray measurements micro-polish was done on the specimen surface.

Frequency of the MBN device used in the experiment was set to 125 Hz and as long as frequency do not manipulated depth of the residual stress measurement remains still. Also, the MBN method is stochastic [24], i.e., the electronic envelope is never the same with another envelope taken under the same conditions of external magnetization. Even the same conditions of magnetization is satisfied, magnetic microstructure of a ferromagnetic grain is never be the same.

CHAPTER 6

CONCLUSIONS

This study reveals the effect of successive weld passes on the surface residual stress state and distortion of the API 5L X-70 steel plates. Two series of the fixed-end and free-end plates were welded by applying 2, 4 and 8 passes for evaluating the complex nature of residual stress and deflection. The longitudinal components of the surface residual stresses were determined non-destructively by Magnetic Barkhausen Noise (MBN) measurements. In order to convert magnetoelastic parameter into residual stress values, a specific calibration procedure was applied. A MBN measurement system having automated scanning ability was used. The MBN measurement results were analyzed and discussed by considering the results of microstructure investigations and hardness measurements. X-Ray diffraction measurements were carried out for verification of the MBN results. The following conclusions can be drawn from this particular study:

1. In the multi-pass welding, each weld pass remarkably affects the microstructure in HAZ and the residual stress state. As number of passes increases amount of angular deflection reduces.

2. Examinations from the front side of the surface reveals that the maximum residual stress exists in the weld zone, close to the weld centerline, and it tends to decrease towards the base metal. The magnitude of the tensile residual stress increases as the number of the weld pass increases. On the back surface, however, increased number of weld-passes leads a reduction in tensile residual stresses. Since there is not any microstructural change on back

side, the stress-relief effect of high heat input due to subsequent weld passes reduces the MBN emission by enhancing the domain wall movement.

3. As the number of weld passes increases, MBN profiles (fingerprints) of both fixed-end and free-end specimens shift to lower values of magnetic field strength and the peak height of the MBN emission increases.

4. With its suitability for static and dynamic measurement, MBN method seems to be an easy and non-destructive way for complete monitoring of surface residual stresses in welded components after an appropriate calibration. It may provide critical information for optimizing weld parameters such as number of weld passes to control residual stress state for a better service performance without early failure.

REFERENCES

[1] API Specifications 5L, Specifications for Line Pipe, forty-fourth ed., American Petroleum Institute, p.108, (2007).

[2] J.G. Williams, Advances in Steels for High Strength Erw Linepipe Application in Australia, Institute of Materials Engineering Australasia Ltd, Materials Forum, Vol. 31, p.1 – 10, (2007).

[3] V.I. Spivakov, E.A. Orlov, P.L. Litvinenko, A.V. Nogovitsyn, Kinetics of Austenite Transformation and Bainite Structure Formation during Strain-Heat Hardening of Low-Perlite Steel X70 (X 65) (API 5L Gr X-60, API 5L Gr X-70) Plates for Gas Pipelines, , Metallurgical and Mining Industry, Vol. 2, No. 1, p.39 – 42, (2010).

[4] A. Carboni, A. Pigani, G. Megahed and S.K. Paul Danieli, Casting and rolling of API X70 grades for arctic applications in a thin slab rolling plant, Millennium Steel International, p.131 – 136, (2008).

[5] K. Yuichi, Overview of Recent Welding Technology Relating to Pipeline construction, Transactions of Joining and Welding Research Institute, Vol. 37, No.1, p.1 – 5, (2008).

[6] S.H. Hashemi, Strength–hardness statistical correlation in API X65 steel, Materials Science and Engineering: A, Vol. 528, Issue.3, p.1648 – 1655, (2011)

[7] P.J. Withers, Residual stress and its role in failure, Reports on Progress in Physics, 70(12), p.2211 – 2264, (2007).

[8] C.L. Tsai, S.C. Park and W.T. Cheng, Welding Distortion of a Thin-Plate Panel Structure - The effect of welding sequence on panel distortion is evaluated, Welding Research Supplement, p.157 – 165, (1999).

[9] I. Sattari-Far, M.R. Farahani, Effect of the weld groove shape and pass number on residual stresses in butt-welded pipes, International Journal of Pressure Vessels and Piping Vol.86, p.723 – 731, (2009).

[10] J. Gauthier , T.W. Krause, D.L. Atherton, "Measurement of Residual Stress in Steel Using the Magnetic Barkhausen Noise Technique", NDT&E International, Vol. 31, No. 1, p. 23-31, (1998).

[11] N.S. Rossini, M. Dassisti, K.Y. Benyounis, A.G. Olabi, Methods of measuring residual stresses in components, Materials and Design, Vol. 35, p. 572 – 588, (2012).

[12] C.H. Gür, İ. Çam, Comparison of magnetic Barkhausen noise and ultrasonic velocity measurements for microstructure evaluation of SAE 1040 and SAE 4140 steels, Materials Characterization, Vol. 58, p. 447 – 454, (2007).

[13] E.J. McDonald, K.R. Hallam, W. Bell, P.E.J. Flewitt, Residual stresses in a multi-pass CrMoV low alloy ferritic steel repair weld, Materials Science and Engineering: A vol.325, issue 1-2, p.454 – 464 (2002).

[14] D. Deng, H. Murakawa, Numerical simulation of temperature field and residual stress in multi-pass welds in stainless steel pipe and comparison with experimental measurements, Computational Materials Science, Vol.37, Issue 3, p.269 – 277, (2006).

[15] Z. Zeng, L. Wang, P. Du, X. Li, Determination of welding stress and distortion in discontinuous welding by means of numerical simulation and comparison with experimental measurements, Computational Materials Science, Vol.49, Issue 3, p.535 – 543, (2010).

[16] C. Jagadish, L. Clapham, D.L. Atherton, Influence of Uniaxial Elastic Stress on Power Spectrum and Pulse Height Distribution of Surface Barkhausen Noise in Pipeline Steel, IEEE Transactions on Magnetics, Vol. 26, No:3, p.1160 – 1163, (1990).

[17] S. Tiitto And S. Saynajakangas, Spectral Damping in Barkhausen Noise, IEEE Transactions on Magnetics, Vol. Mag-11, No: 6, p.1666 – 1672, (1975).

[18] L. Clapham, T.W. Krause, H. Olsen, B. Ma, D.L. Atherton, P. Clark and T.M. Holden, Characterization of texture and residual stress in a section of 610 mm pipeline steel, NDT & E Int. Vol.28, Issue 2, p73 – 82 (1995).

[19] K. Mandal, M.E. Loukas, A. Corey, D.L. Atherton, Magnetic Barkhausen noise indications of stress concentrations near pits of various depths, Journal of Magnetism and Magnetic Materials Vol. 175, p.255 – 262, (1997).

[20] O. Saquet, J. Chicois, A. Vincent , Barkhausen noise from plain carbon steels: analysis of the influence of microstructure, Materials Science and Engineering: A, Vol. 269, Issues 1 – 2, p.73 – 82, (1999).

[21] J. Anglada-Rivera, L.R. Padovese, J. Capo-Sanchez, Magnetic Barkhausen Noise and hysteresis loop in commercial carbon steel: influence of applied tensile stress and grain size, Journal of Magnetism and Magnetic Materials, Vol.231, Issues 2 – 3, p.299–306, (2001).

[22] S. Desvaux, M. Duquennoy, J. Gualandri, M. Ourak, The evaluation of surface residual stress in aeronautic bearings using the Barkhausen noise effect, NDT&E International, Vol. 37 p. 9 –17, (2004).

[23] I. Mészáros, Micromagnetic Measurements and Their Applications, Materials Science Forum, Vols. 414 – 415, p. 275-280, (2003).

[24] K. Sapountzi, Residual stress prediction in welds via the Barkhausen Noise Technique, Key Engineering Materials, Vol. 495, p. 209 – 212, (2012).

[25] H.I. Yelbay, Determination of Residual Stress State in Steel Weldments, M.s Thesis, METU (2009).

[26] M. Bruns, T. Nitschke-Pagel, Determination of Welding Residual Stresses with help of the Micromagnetic Measurement Method, Materials Science Forum, Vols. 524-525, p. 647 – 652, (2006).

[27] T. Nitschke-Pagel, K Dilgerand, H Eslami-Chalandar, Determination of residual stresses in welded structural steels with help of micromagnetic measurements, Materials Science Forum Vol. 681, p. 194 – 201 (2011).

[28] C. Kownacki, The application of multiparametric analysis of Barkhausen noise using continuous wavelet transform in comparative stress testing, Nondestructive Testing and Evaluation, 23:2, p.99 – 107, (2008).

[29] K. Kolařík , N. Ganev, J. Jersák, Application of X-Ray Diffraction And Barkhausen Noise Analysis For Stability Control During Machining, Materials Engineering - Materiálové inžinierstvo 18 p.49-56, (2011).

[30] G. Totten, M. Howes, T. Inoue, Handbook of residual stress and deformation of steel, Materials Park, Ohio, ASM International, p.3, (2002).

[31] P.J. Withers, H. K. D. H. Bhadeshia, Residual stress Part 2 – Nature and origins, Materials Science and Technology, Vol. 17, p.366 – 376, (April 2001).

[32] K. Masubuchi, Residual stresses and distortion in welds, Encyclopedia of Materials Science and Technology, p.8121 – 8123, (2003).

[33] E. Macherauch, K.H. Kloos, Origin, Measurements and Evaluation of Residual Stresses. Residual Stresses in Science and Technology, DGM Inform Verlag, p.3-26 (1987).

[34] A. Sluzalec, Theory of Thermomechanical Processes in Welding, Springer (1st edition), p.148, 158, 159, (June, 2005).

[35] P.J. Withers, H. K. D. H. Bhadeshia, Residual Stress Part 1 – Measurement Techniques Materials Science and Technology Vol. 17 p.355 – 365, (April 2001).

[36] S. Chikazumi , "Physics of Magnetism", Wiley, New York, p.113 – 127 (1997).

[37] S. Desvaux, M. Duquennoya, J. Gualandri, M. Ouraka, The evaluation of surface residual stress in aeronautic bearings using the Barkhausen noise effect, NDT&E International 37, p.9 – 17, (2004).

[38] J. C. McClure, K. Schroeder, The Barkhausen Effect, CRC Critical Reviews of Solid State Science, 6, p.45 (1976).

[39] ASM Metals Handbook vol.17 – Nondestructive Evaluation and Quality Control, 9th edition, p.317 – 320, (1989).

[40] P.S. Neelkanta, Handbook of Electromagnetic Materials: Monolithic and Composite Versions and Their Applications, CRC Press, p.319 – 344, (1995).

[41] B.D. Cullity, Introduction to magnetic materials. London: Addison-Wesley, p.190 – 259, (1972).

[42] Z.D. Wang, Y. Gu, Y.S. Wang, A review of three magnetic NDT technologies, Journal of Magnetism and Magnetic Materials Vol. 324, p.382 – 388, (2012).

[43] S. Tiitto, On the influence of microstructure on magnetization transitions in steel, Acta Polytechnica Scandinavia, Appl. Phys. Series Vol. 119, p.0 –80, (1977).

[44] R. Langman, Some comparisons between the measurement of stress in mild steel by means Barkhausen noise and rotation of magnetization NDT Int., Vol.20, Issue 2, p.93 – 99, (1987).

[45] H. Kwun and G.L. Burkhardt, Effects of Grain Size, Hardness and Stress on the Magnetic Hysteresis Loops of Ferromagnetic Steels, J. Appl. Phys., Vol 61, p.1576, (1987).

[46] A. Alvarez-Rosario, L.R. Padovese, Principal Component analysis and discriminant analysis as a supervised pattern recognition tool for classification of AISI 420 steel samples subjected to a different heat treatment using Magnetic Barkhausen Noise signals, 18th World Conference on Nondestructive Testing, Durban, South Africa, (16-20 April 2012).

[47] K. Davut, Characterization of Steel Microstructures by Magnetic Barkhausen Noise Technique, M.s Thesis, METU (2006).

[48] I. C. Noyan, J. B. Cohen, Residual Stress Measurement by Diffraction and Interpretation, Springer-Verlag, New York, p.110, (1987)

[49] ASTM E 112 – 96, Standard Test Methods for Determining Average Grain Size, p.7 – 9, (2004).